Doc-CR-85-001

SPAR R.1188 ISSUE A

(2)

MODAL TEST OF T-SAT

SPAR

SPAR R.1188 **ISSUE** A

(2)

MODAL TEST OF T-SAT

PREPARED BY (1) Sherry Draisey

REASON FOR RE-ISSUE

DATE November, 1984

APPROVALS

P.J. Smith Group Leader Structures	P.J. Smith
A.S. Jones Manager, Mechanical Engineering	
P.A. McIntyre Director, Engineering	P.A. McIntyre

AMENDMENTS

NUMBER	REASON FOR AMENDMENT	SIGNATURE	DATE

Spar Aerospace Limited
Remote Manipulator Systems Division
1700 Ormont Drive, Weston, Ontario, Canada M9L 2W7

SPAR Space & Electronics Group

TEL (416) 745-9680 TELEX 065-27360 SPARORM TOR TWX 610-491-1503 CABLE-SPARORM TOR

Government of Canada / Gouvernement du Canada

Department of Communications

DOC CONTRACTOR REPORT DOC-CR-85-001

DEPARTMENT OF COMMUNICATIONS - OTTAWA - CANADA

SPACE PROGRAM

TITLE: MODAL TEST OF T-SAT

AUTHOR(S): Sherry Draisey

ISSUED BY CONTRACTOR AS REPORT NO: SPAR R.1188

PREPARED BY: SPAR Aerospace Limited
Remote Manipulator Systems Division
1700 Ormont Dr.
Weston, Ontario
M9L 2W7

DEPARTMENT OF SUPPLY AND SERVICES CONTRACT NO: 01ST.36001-2-1794
Serial No. 1ST82-00137, Phase II

DOC SCIENTIFIC AUTHORITY: Dr. F.R. Vigneron

CLASSIFICATION: Unclassified

DATE:

SPAR-RMS-R.1188
ISSUE A

ABSTRACT

MODAL TEST OF T-SAT

by

S. Draisey

This report describes the modal test of a structure (referred to as T-Sat) designed to represent a simplified version of the primary structure of a communications satellite. It constitutes the second phase of work being done at RMSD on the development of modal testing of aerospace structures.

Several modal test techniques, within the category of phase separation methods, were used to obtain the modal parameters. Two structures were tested independently and then combined to form the coupled T-Sat structure. The data from the tests were to be supplied for use in a substructure coupling exercise. The requirement of an experimental data base was a significant extension to experimental modal work being done within the Canadian Aerospace community.

A brief description of the substructure work and results are also included within this report.

TABLE OF CONTENTS

TABLE OF CONTENTS - Continued

LIST OF FIGURES

LIST OF FIGURES - Continued **PAGE**

LIST OF TABLES

LIST OF TABLES - Continued

LIST OF APPENDICES

LIST OF SYMBOLS

a	Acceleration
f	Frequency
h(w)	Unit impulse response function
H(w)	Frequency response function
$\gamma^2(f)$	Coherence function
ϕ	Eigenvector or mode shape coefficient
w	Frequency = $2\pi f$
x	Displacement in time domain
X	Displacement in frequency domain

1.0 INTRODUCTION AND OBJECTIVES

The work described in this report has been funded under D.S.S. Contract 01ST.36001-2-1794, S/N 82-00137, Phase II. It covers the objectives described in contract amendment #4, July 1983. In summary, the objectives included:

(a) Extend modal technique developed in Phase I to include techniques applicable to the satellite class of structures - in particular, investigate:

i) mini-shaker (single point) force input
ii) impact hammer input
iii) free-free test configuration

(b) Provide modal data suitable for use in substructure coupling software, SYSTAN. The data was to be such that it could be used to evaluate the SYSTAN software (under a separate parallel contract) as a tool in spacecraft structural design.

Implicit in this objective was the test of two independent structures which would subsequently be physically coupled and tested as a unit.

(c) Develop a technique to extend modal software to process base input excitation.

The parallel contract mentioned in (b) was a part of an ARAD contract. The work was performed by the SAS Division of Spar and is described in Reference 6.

Substructure coupling analysis is a structural technique which combines the modal characteristics of two or more independent structures to predict the results of the equivalent physical combination. The technique can be applied using modal characteristics of the individual structures determined either analytically (Finite Element Model) or experimentally (Modal Test).

Obvious examples for substructure coupling in aerospace structures include:

(a) The primary structure as one structure and the antennae as a substructure to be coupled to it.

(b) Payloads and manipulators coupled to the space shuttle.

Such a definitions of subsystems makes sense physically as well as contractually. It is quite standard for two different contractors to build the two units. Each of the contractors can determine the modal characteristics of

their structure individually and the overall, combined response can be determined from the substructure coupling analysis.

To provide data to investigate substructure coupling using an experimental data base, a structure known as T-Sat was tested. A secondary structure was also built and tested. The two structures were then joined together (by 3 bolts and a linear spring) and tested.

An excerpt of the coupling results (reported in Reference 6) is included in Table 1-1. These results were based on the experimental modal work described in this report. The NASTRAN results, included as part of the substructure exercise were updated to reflect the modal parameters and shapes described in Section 5.

The extension of modal analysis techniques to base excitation is an important one to the aerospace community.

A base driven test simulates the load path seen by structures in a launch configuration, and that of appendages (solar arrays or antennas) mounted to a spacecraft in a deployed configuration. In conventional modal tests, it is sometimes necessary to drill holes in the structure to excite internal modes. Base excitation eliminates that requirement.

The base configuration is also used by some aerospace prime contractors as an efficient means of obtaining analytical dynamic structural properties from subcontractors. Thus it is desirable to be able to provide experimental results in the same form.

This report includes the small software change needed to process modal data from a base excitation test, as well as a comparison of base results to that of a more conventional single point mini-shaker test.

TABLE 1-1

COMPARISON OF SUBSTRUCTURE COUPLING RESULTS

MODE NO.	TEST RESULTS COUPLED STRUCTURE (Hz)	UPDATED NASTRAN PREDICTIONS (Hz)	SYSTAN COUPLING FEM DATA BASE (Hz)	SYSTAN COUPLING EXPERIMENTAL DATA BASE (Hz)
1	15.1	14.5	16.9	12.1
2	23.5	24.5	25.4	23.7
3	26.6	26.4	27.1	26.7
4	28.0	27.6	-	30.2
5	32.0	30.0	28.7	-

2.0 DESCRIPTION OF STRUCTURE

The T-Sat primary structure was designed and built under an RMSD internal R & D activity. Its purpose was associated with the manufacture of a composite structure of this configuration. Thus it was not purpose-built for these tests. It represents a very simplified scaled version of a thrust tube and equipment shelf configuration. The structure is somewhat non-linear and highly antisotropic.

The T-Sat secondary structure was designed specially for the coupling exercise. The structure was very simple to model analytically and to test.

The type of interface connections to be made to the primary structure were designed to thoroughly investigate the limits of substructure coupling techniques.

Figure 2-1 illustrates the two structures and the types of interface connections between them.

2.1 PRIMARY STRUCTURE

Figure 2-2 shows a photograph of the primary structure, mounted to the 40^K Vibration shaker table, complete with accelerometer instrumentation.

The primary structure consisted of a carbon composite 'thrust cone', a single 40" diameter shelf of balsa core with aluminum face sheets, four aluminum struts between the shelf and an aluminum flange around the thrust cone. The strut connections were pins. To bring the structural frequencies into the range typical of communication satellite primary structures, masses were added to the shelf. Eight were added around the outer edge of the shelf and one was added to the underside of the centre of the shelf. Table 2-1 lists the mechanical parameters of the primary structure:

2-2 SECONDARY STRUCTURE

Figure 2-3 shows a photograph of the secondary structure, suspended upside down from 3 bungie cords, in preparation for a free-free impact hammer test. (complete with accelerometer instrumentation).

The secondary structure was essentially a flat aluminum plate. It was approximately triangular in shape, with an offset flange welded to one end.

Table 2-2 lists the dimensions of the secondary structure.

2.3 COUPLED STRUCTURE

The coupled structure consisted of the primary and secondary structures joined together.

Figure 2-4 shows a picture of the secondary structure attached to the shelf of the primary structure (complete with instrumentation).

The interface connections between the two structures consisted of:

(a) Three bolts through secondary structure flange and primary structure shelf.

(b) Linear one degree of freedom spring between tip of secondary structure and primary structure shelf.

The total weight of the coupled structure was 49.1 lb. The first natural frequency was approximately 15 Hz.

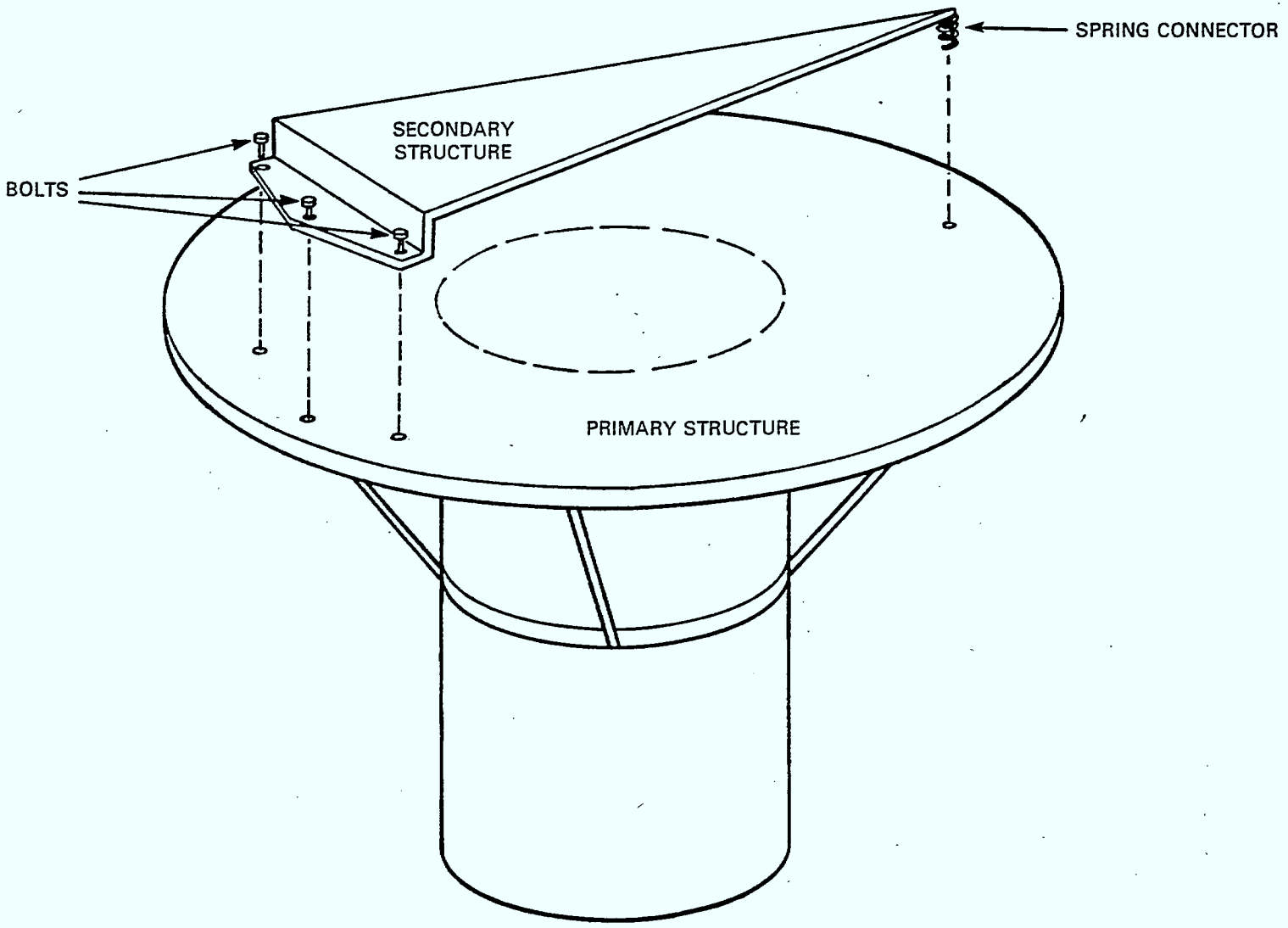

FIGURE 2-1 T-SAT STRUCTURE

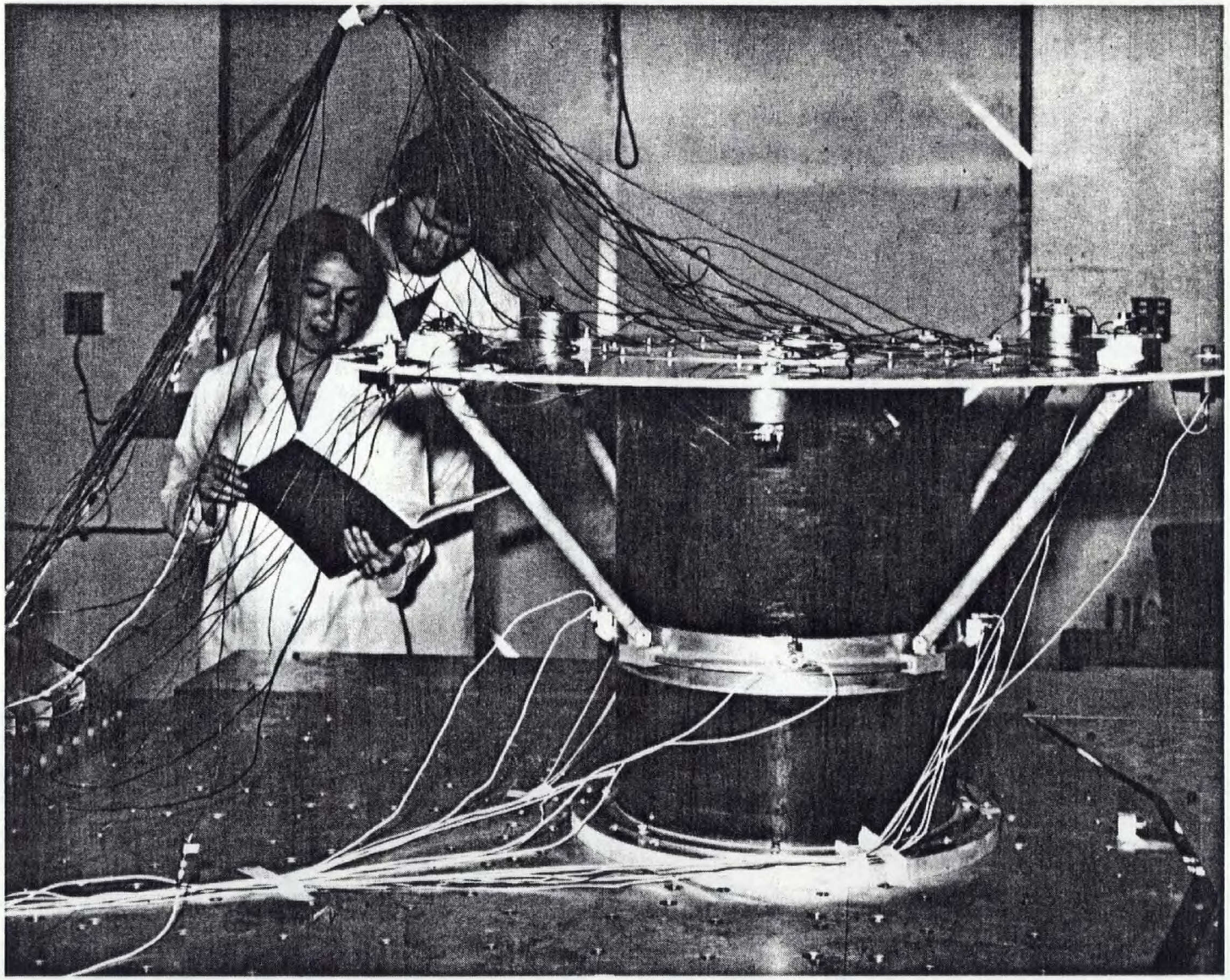

FIGURE 2-2 PICTURE OF THE PRIMARY STRUCTURE

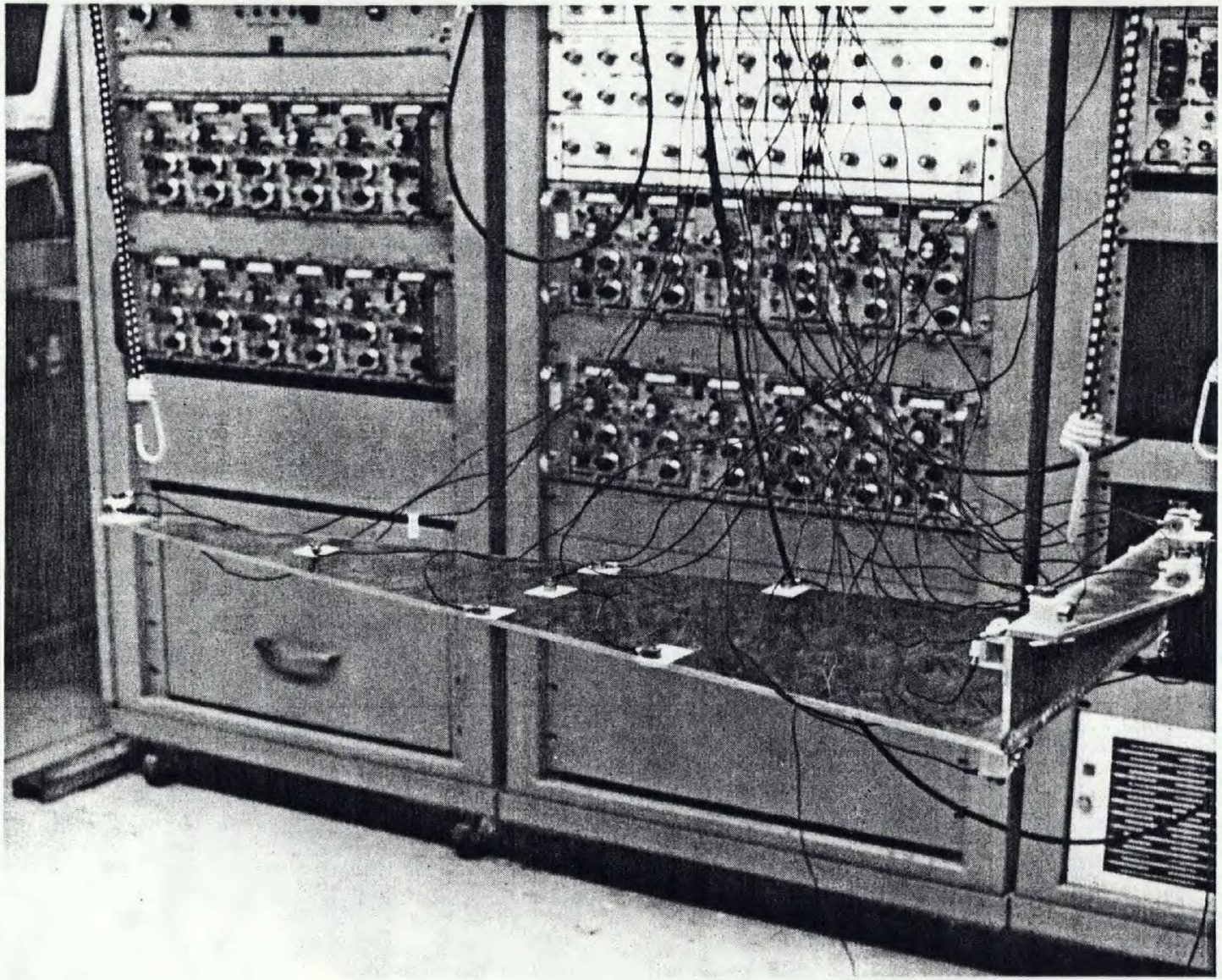

FIGURE 2-3 PICTURE OF THE SECONDARY STRUCTURE

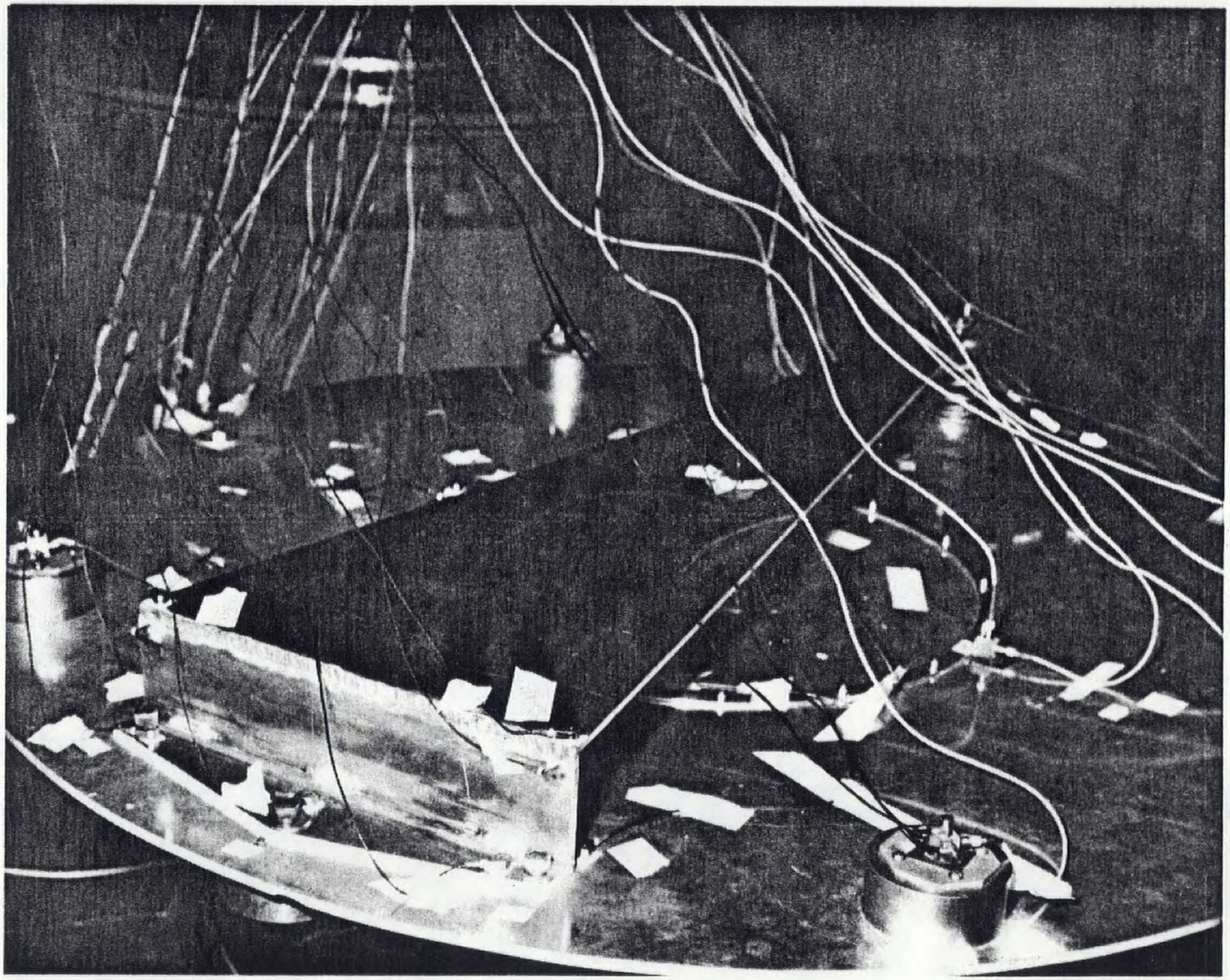

FIGURE 2-4 PICTURE OF COUPLED STRUCTURE, SHELF AND SECONDARY STRUCTURE

TABLE 2-1

MECHANICAL PARAMETERS - PRIMARY STRUCTURE

	WEIGHT	DIMENSIONS	MATERIAL
SHELF:	4.78 LB.	diameter: 40" 2 Sheets; .020" thick .25" thick	 Aluminum Balsa
ADDED MASSES:			Brass
Centre Mass	7.80	Diameter:	
8 Outer Masses, each	2.67	Diameter: 3"	
STRUTS (each)	.39	.75" O.D. .0625" thick	Aluminum
THRUSTCONE		diameter: 15" height : 21" thickness: .080"	Carbon Composite
THRUST CONE MID FLANGE		thickness: .25"	Aluminum
THRUST CONE BASE FLANGE		thickness: .125"	Aluminum

The total weight of the structure was 43.2 lb. The first resonant frequency of the structure was about 20 Hz.

TABLE 2-2

SECONDARY STRUCTURE DIMENSIONS

SECONDARY STRUCTURE	DIMENSIONS		
	LENGTH	WIDTH	THICKNESS
Plate	33.6"	15.8"	.1875"
Offset Plate	-	15.8"	.1875"
Flange	3.3"	15.8"	.1875"

The total weight of the structure was 5.4 lb. and its first (free-free) natural frequency was about 30 Hz.

3.0 MODAL TESTING CONFIGURATIONS

This section describes the modal testing hardware and software available for the test as well as the options available to establish the test configurations subsequently used for the secondary, primary and coupled structures.

3.1 DESCRIPTION OF TEST FACILITY

The testing was done in the David Florida Laboratory Environmental Test Facility. This vibration lab has primarily been used for acceptance and qualification testing of aerospace structures. It is being upgraded to include a modal test capability.

The modal testing done within this contract has been designed to utilize the existing facilities and to determine where improvements should be made. The base excitation testing exercises were initiated because of the strength that the laboratory has in vibration shaker tables (there are 4 in the lab, of various sizes).

The mini-shakers and force transducers were purchased within this contract, to allow investigation of the conventional (within modal testing) single point excitation techniques.

3.1.1 MODAL TESTING HARDWARE - Figure 3-1 is a schematic of the vibration test configuration for a mini-shaker test of the T-Sat primary structure. For the impact hammer test, the impact hammer replaced the mini-shaker, amplifier and control system. For the base acceleration input test of the primary structure the mini-shaker, the force transducer was eliminated and the HP system controlled the 40^K shaker table.

3.1.1.1 Control System - The DFL vibration facility is equipped with two vibration control systems; a HP 5427A system and a Gen Rad 2503. Both systems are capable of sine sweep and random testing - open or closed loop.

The HP5427A was the control system used to run the base excitation tests - in a closed loop mode. The mini-shaker testing was done using open loop random excitation generated by the Gen Rad 2503 system.

3.1.1.2 Excitation Systems - There were three excitation systems used for the T-Sat modal test exercise:

(a) Impact (or Impulse) Hammer. An impulse hammer is a hammer with a force transducer within the head which allows measurement of the force delivered to the structure. The selection of various hammer tips provides some qualitative control to the frequency content of the pulse. The hammer used was a PCB Model 086A03.

(b) A 40,000 lb. electrodynamic exciter was used to provide base acceleration input. The primary structure was bolted to the shaker table.

(c) A portable 100 lb. force mini-shaker (bVTS100/PSA-2X) was used to provide single point force excitation input.

3.1.1.3 Seismic Mass - A seismic mass was built to mount the structure to for the mini-shaker testing.

Tests of the seismic mass indicated that its dynamic characteristics were not suitable (minimum rigid body frequency was too high and first flexible modes were too low in frequency). Reference 2 describes the dynamic characteristics.

In order to perform the mini-shaker tests, the structure was bolted to the 40^K shaker table, which in turn is fixed to a 200 ton reaction mass. The 40^K shaker system is free of dynamic response from 5-450 Hz.

3.1.1.4 Measurement Systems - Two types of measurement systems were used: accelerometers and force transducers. All output responses were measured with accelerometers and the base input was measured by an accelerometer. The force inputs from the impulse hammer and the mini-shaker were measured with force transducers.

The accelerometers used were piezo electric. Light weight ones were used on the flexible components.

The force transducers used were:

DYTRAN 1051V3 (100 lb. Transducer)

3.1.1.5 Data Storage Devices - The analogue test data was stored on tape. The data from the primary and coupled structures was stored by multiplexing five channels of data onto the 14 track METRA PLEX system. The secondary structure data was stored directly onto a 24 channel system.

After the data was acquired by the Gen Rad system, it was stored digitally on disc as frequency response functions.

3.1.1.6 Computer System - The Gen Rad 2503 system is shown in Figure 3-2 (taken from page 8', Reference 1). It consists of:

(a) 4 channel analogue data acquisition system

(b) Digital processing system

(c) Analogue section to drive an exciter

Within the analogue data acquisition phase the analogue data is acquired in conjunction with software operating on the PDP 11/34.

The digital data can be completely processed using the Gen Rad and PDP 11/34 systems, but to speed up the processing, parameter estimation and mode shape extraction were done on a VAX system.

3.1.2 MODAL TESTING SOFTWARE - The modal analysis (test) software is part of the Structural Dynamic Research Corporation package IDEAS. The processing is accomplished by two pieces of software, DATM and MPLUS.

The conversion of time series data to frequency response function data is done by the DATM software.

The modal parameter estimation and mode shape extraction from the frequency response functions is done by the MPLUS software. Figure 3-3 illustrates principal MPLUS functions. Several parameter estimation algorithms are available within MPLUS. The work described in this report was done using a complex exponential technique known as POLYREFERENCE.

In the initial stages of this contract, Version 7 of Modal Plus was used (Modal PLus includes DATM and MPLUS). During the program Version 8 was released.

Reference 3 describes the operation of the software.

3.2 LOGISTICS OF THE TEST

In planning for a modal test, there are many choices which must be made in establishing the configuration to be used. The overriding criteria should be the accuracy of the results, but time and hardware limitations must be included in the planning.

3.2.1 ACCELEROMETER LOCATIONS - The number of accelerometers used were minimized due to the following factors:

(a) The data acquisition system could only process 4 channels at a time - one channel was the measured input and the other three were accelerometer output channels. Thus each data set of 60 accelerometers required 20 passes through the data - each pass took a minimum of 20 minutes.

(b) The number of accelerometers available for the test was limited. The laboratory is equipped with 200 accelerometers, but only about half of those were suitable with respect to size and frequency range. Of the remaining 100, 20 had been sent to B.A.e to instrument the L-Sat primary structure model. The vibration lab needed about 20 for its day to day testing.

(c) The analogue data storage device, a multiplex system, known as Metraplex, could not accommodate more than 70 data channels.

The accelerometer locations chosen were an attempt to maximize the number of mode shapes which could be interpreted for the minimum number of accelerometers. In fact, probably twice as many accelerometers should have been used.

The decision to instrument the entire primary structure, rather than assume symmetry and only instrument half or a quarter of it was justified by the results. The symmetry of the structure provided a level of redundancy which was useful when an accelerometer channel was of poor quality. The impact of non isotropic nature of balsa core was not fully appreciated prior to the test.

The test results showed that the structure did not exhibit all of the symmetry initially expected.

3.2.2 BOUNDARY CONDITIONS - A free-free test involves suspending the structure from very soft supports - e.g. bungie cords. The resonant frequency of the supports must be significantly lower than that of the structure.

A fixed-free test implies that one end of the structure is rigidly attached to ground while the other is free of any support constraints (e.g. a cantilever configuration). The resonant frequency of the support structure must be significantly higher than that of the structure.

There are practical limitations to the accuracy of both configurations. The fixed-free configuration is usually more representative of the load path that the structure will experience in use, but the assumption of a fixed boundary is not possible to actually realize.

Both types of boundary conditions were used within this contract: free-free for the secondary structure and fixed-free for all other tests.

3.2.3 TEST EXCITATION METHODS - The types of test excitation methods which are used for modal testing can be grouped into two categories - steady state and transient.

The steady state methods include sine or random input; force or acceleration (base). A random test takes less time for the test itself, as well as the data acquisition.

The transient inputs include:

(a) step relaxation (low frequency method)
(b) impact hammer (high frequency method)
(c) acceleration shock load.

The inputs can be at one point (single point excitation) or at several points (multi-point excitation). Multipoint input is recognized as being the better form of input because it can give a better distribution of forces and it reduces the problem of adequate excitation to all modes. Single point input can be repeated several times at different times, but the test time increases significantly and problems of non-stationarity can seriously distort the results.

Both of the steady state methods were used within this test program, as well as one transient input (impact hammer).

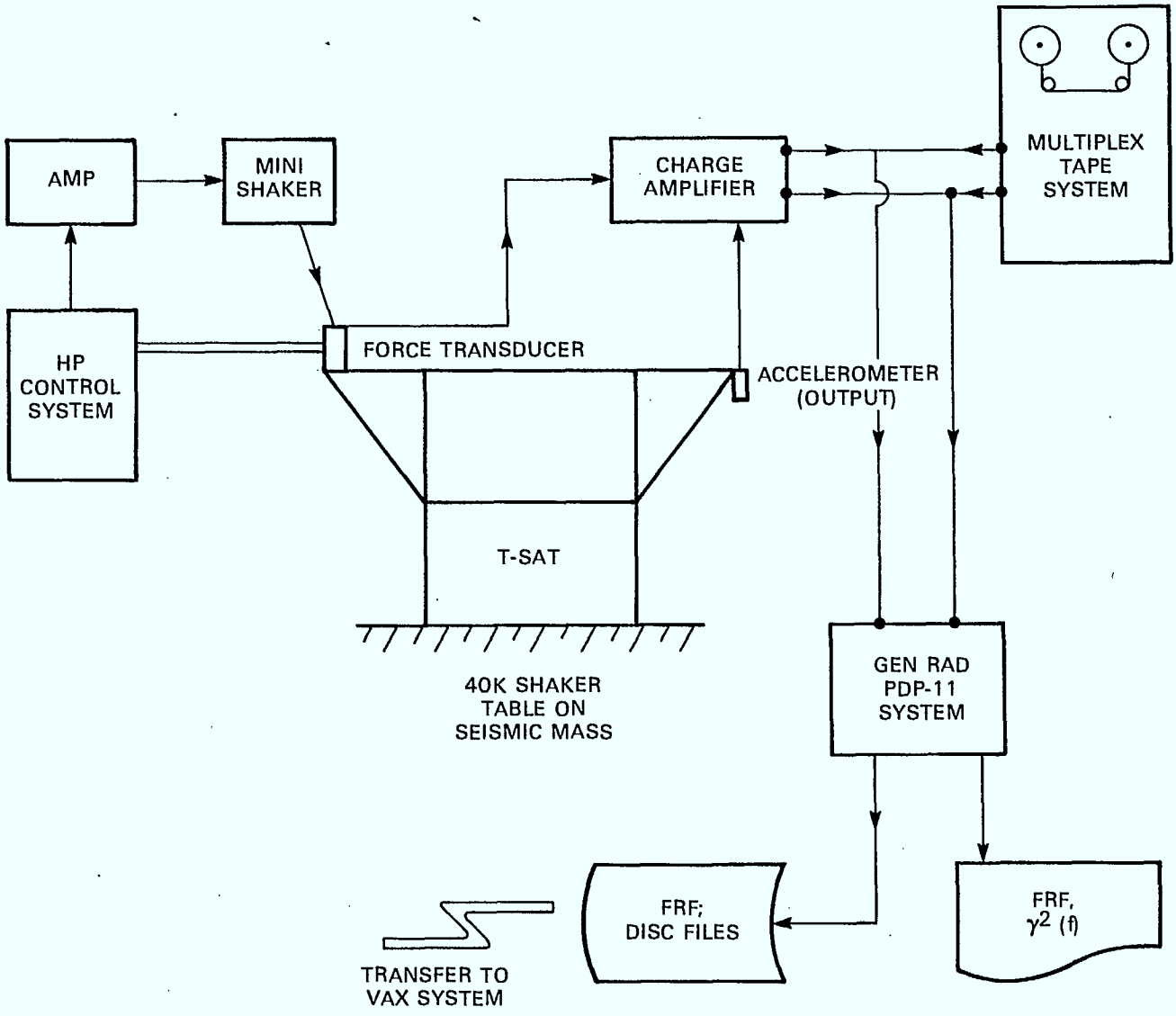

FIGURE 3-1 HARDWARE SCHEMATIC

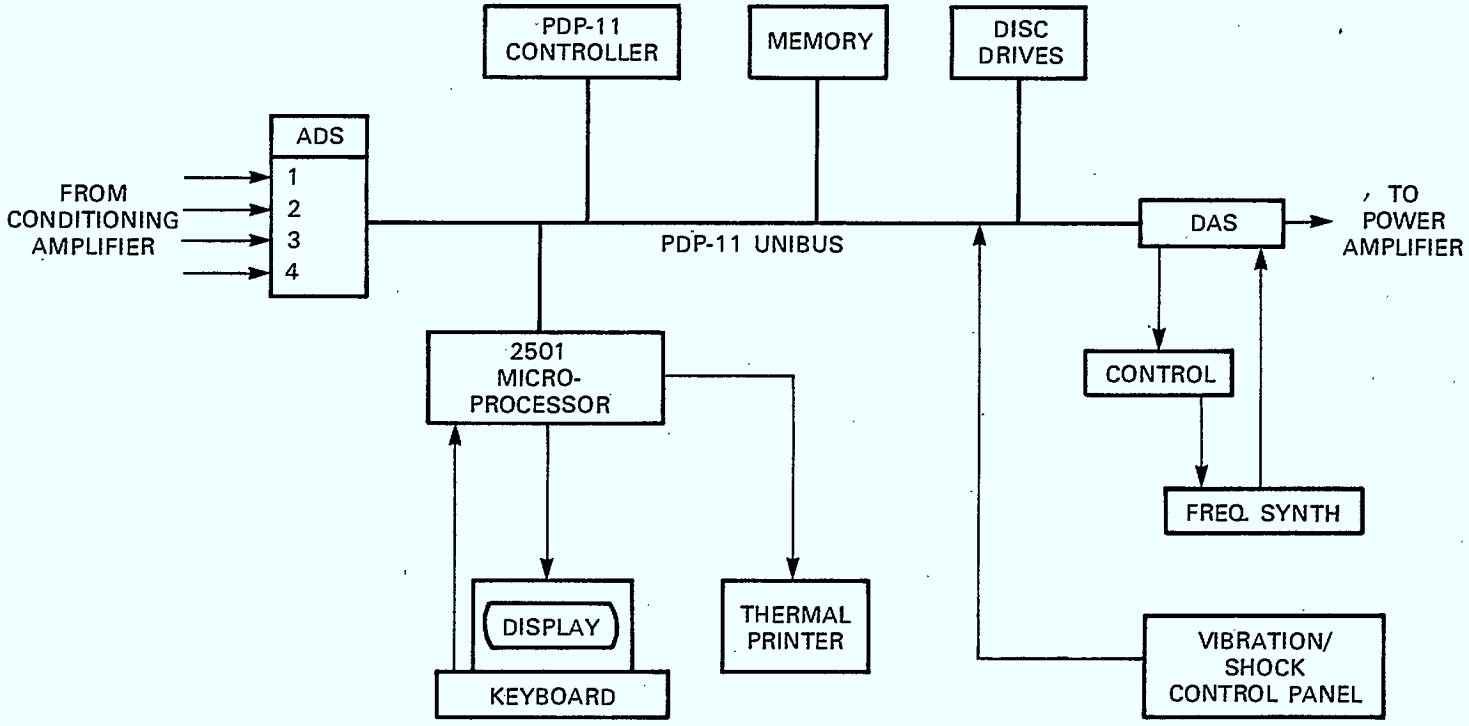

FIGURE 3-2 GEN RAD 2503 SYSTEM

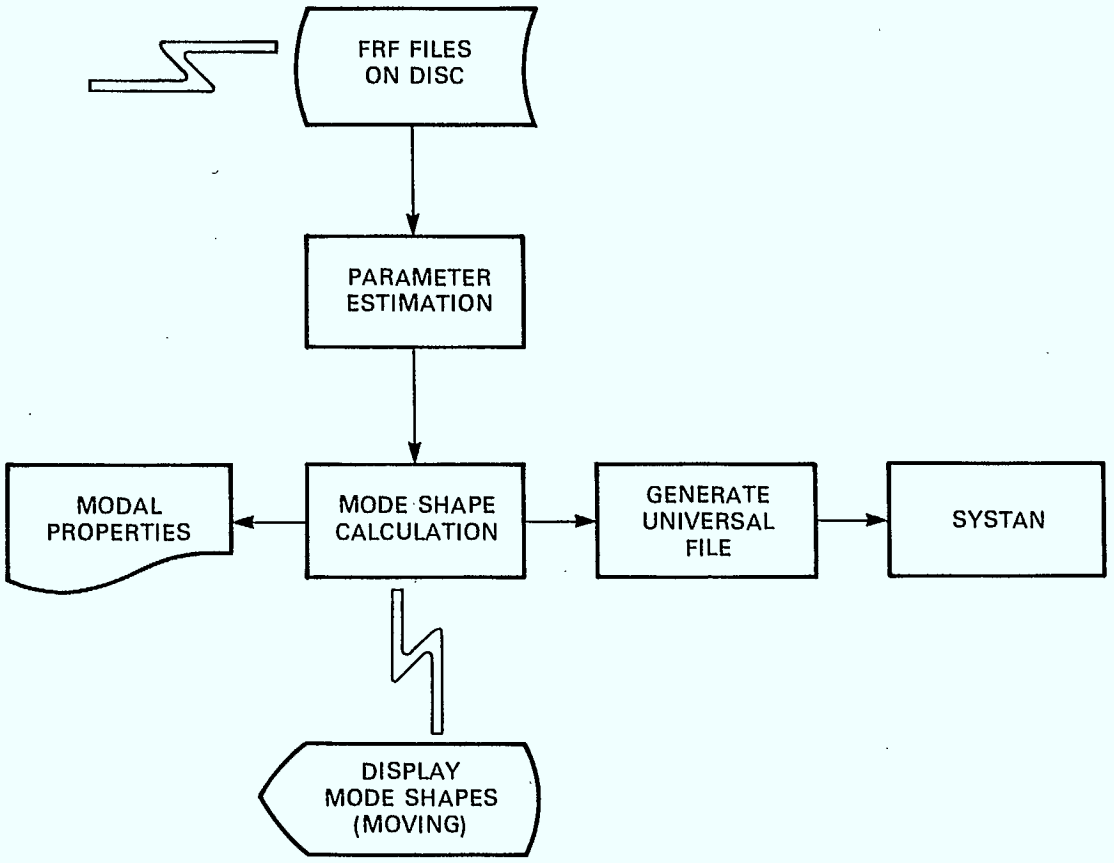

FIGURE 3-3 MPLUS SOFTWARE PROCESSING

4.0 IMPACT TEST OF SECONDARY STRUCTURE

The secondary structure was tested using a free-free test configuration with impact hammer excitation. The configuration choice was based on three facts:

(a) Impact hammer testing is well suited to simple, linear, lightly damped structures.

(b) The substructure coupling software to be used for the subsequent analysis required that the modes of the interfacing structure be in a free-free format.

(c) The configuration had not been used in any other phase of this contract.

4.1 TEST CONFIGURATION

Initially the secondary structure was suspended from bungie cords, attached to the structure via 2" pieces of fine wire at each of the three suspension points.

Figure 4-1 indicates the configuration and the measurement degrees of freedom.

By comparison with the FEM of the structure, it was determined that the wire connections were causing problems. Elastic bands were substituted to correct the problem.

The structure was tested using 7 different impact points:

21 X
22 X
23 Y
23 Z-
24 Z-
26 Z-
36 Z-, four impacts averaged for each point.

4.1.1 SECONDARY STRUCTURE ACCELEROMETER LOCATIONS - The secondary structure was instrumented with 26 accelerometers (maximum number that could be stored on the conventional tape deck system was 24. The two additional channels were taken 'live' and not stored on analogue tape).

Figure 4-1 shows the accelerometer degrees of freedom. Figure 4-2 shows the geometry coordinates. The following is a list of the coordinates. (in inches)

	X	Y	Z
20	-16.75	5	21.238
21	-18.25	0	21.238
22	-16.75	-5	21.238
23	17.75	0	24.238
24	-16.0	-5.75	21.238
25	-16.0	5.75	21.238
26	-16.0	-5.75	24.238
27	-16.0	5.75	24.238
28	- 6.0	-4.0	24.248
29	- 6.0	+4.0	24.238
30	0	-3.0	24.238
31	0	+3.0	24.238
32	8.75	0	24.238
36	0	0	24.238

The subsequent substructure analysis required that the interface points of the secondary structure be instrumented in three degrees of freedom - thus the high concentration of accelerometers in the flange area.

4.2 TEST RESULTS

The test results of the secondary structure include frequency response and coherence functions of one of the two (out of 7 possible) impact points chosen to do base parameter estimation on. The parameter estimation method used was the POLYREFERENCE technique. Fifty-two frequency response functions were used to estimate the parameters (26 points times the two impact points).

4.2.1 FREQUENCY RESPONSE FUNCTIONS - Figure 4-3 is a frequency response function taken from point 24Z (flange end of structure (excited by impact at point 36Z (centre of triangular plate section). The maximum rigid body mode of the structure (non-zero frequency due to the presence of the bungie cords) was at 2.3 Hz.

Examination of the frequency response function indicates the presence of 7 resonant peaks and 3 deep valleys (anti-resonances).

The coherence function shown in Figure 4-4 is equal to 1 except in the regions of the anti-resonances.

In fact the secondary structure has 17 resonances between 10-450 Hz. There are two reasons why only 7 show on the frequency response function shown in the

figure. Some of the modes are very closely spaced and only appear as one peak. Other modes may have almost no response amplitude at the accelerometer location 24Z.

Figure 4-5 is a reciprocity check between the frequency response of point 36Z excited at point 24Z, and the frequency response of point 24Z excited at point 36Z. The amplitude levels vary slightly. There is phase lag between the two functions of 180° due to the sign change at the excitation point (36Z-).

A reciprocity check is a check on the linearity of the structure. The POLYREFERENCE parameter estimation algorithm depends heavily on the linearity of the structure. If a slight resonant frequency shift occurs between frequency response functions, POLYREFERENCE sees it as two resonances rather than one.

4.2.2 PARAMETER ESTIMATION - Table 4-1 is a list of the roots predicted by POLYREFERENCE. The estimation was done assuming complex residues and also using real residues. The real residues produced the best curve fit, shown in Figure 4-6. There are a large number of 'numerical' roots predicted. The obvious 'numerical' roots are those which have; very high damping, phase shifts of zero or 2 and frequencies outside the range of available data.

Data for the secondary structure was filtered out above 450 Hz. Table 4-2 is a list of the selected parameters. The curve shown in Figure 4-6 has been generated from the selected parameters.

Figure 4-7 is the curve fit generated from the selected parameters, with a residual correction factor added. It has improved the appearance of the curve below the first resonance but has deteriorated the best fit over some other regions of the curve (particularly the phase).

4.2.3 MODE SHAPES - Figures 4-8 and 4-9 show the first and second bending modes, taken directly from the experimental results.

Figure 4-10 shows the results of the modal assurance criteria check for redundant resonances. Modes 17 and 18 are obviously redundant modes. The criteria cannot obviously eliminate any other modes, but closer scrutiny of modes 8, 9 and 13 indicate that they have damping significantly higher than the other modes.

It is not clear if modes 8, 9 and 13 are actually physical resonances or just numerical aberrations.

Table 4-3 lists the modes, modal mass (normalized to a maximum displacement of 1) and gives a description of the shape. The modal mass can not exceed the mass of the structure (1.4×10^{-2}). This criteria casts suspicion on modes 5, 8, 10, 12 and 14.

4.3 DISCUSSION OF RESULTS

The impact hammer test results, at the frequency response function level, were very good. This is generally the case for simple linear, lightly damped structures. Even with good frequency response function data, it was not possible to conclusively eliminate all potential 'numerical modes' generated by the Polyreference software.

The free-free boundary condition used for this test was not as easy to achieve as had been anticipated. Without the aid of an FEM, erroneous results would have been obtained. Conversely, the FEM produced highly erroneous results in the first iteration (for torsion modes), which would not have been discovered without the modal test. The free-free test configuration was chosen because the substructure coupling program, (for which the data was intended), could only operate on free-free boundary conditions.

The estimate of modal mass is based on the results of one frequency response function. Considering the importance of modal mass in substructure coupling, and the aid modal mass offers in eliminating spurious modes, it would be advisable to develop an averaging technique to estimate it.

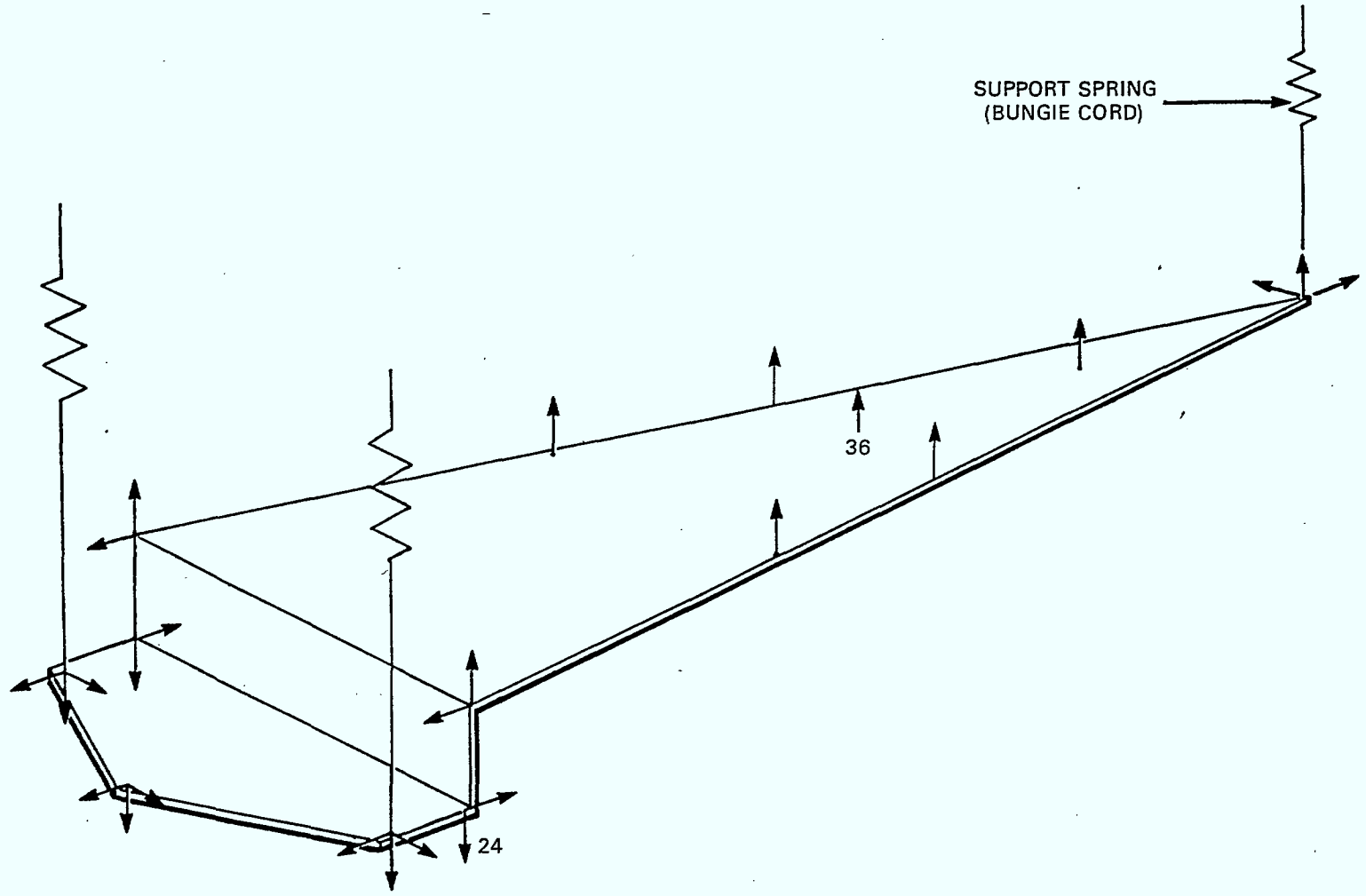

FIGURE 4-1 SECONDARY STRUCTURE INSTRUMENT CONFIGURATION

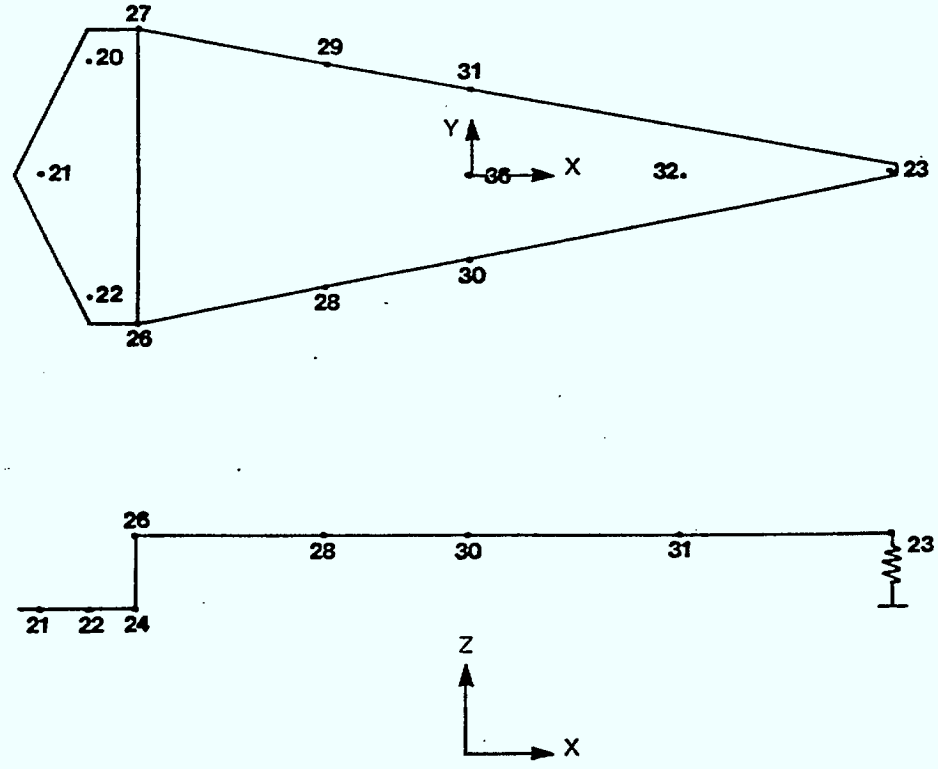

FIGURE 4-2 SECONDARY STRUCTURE GEOMETRY

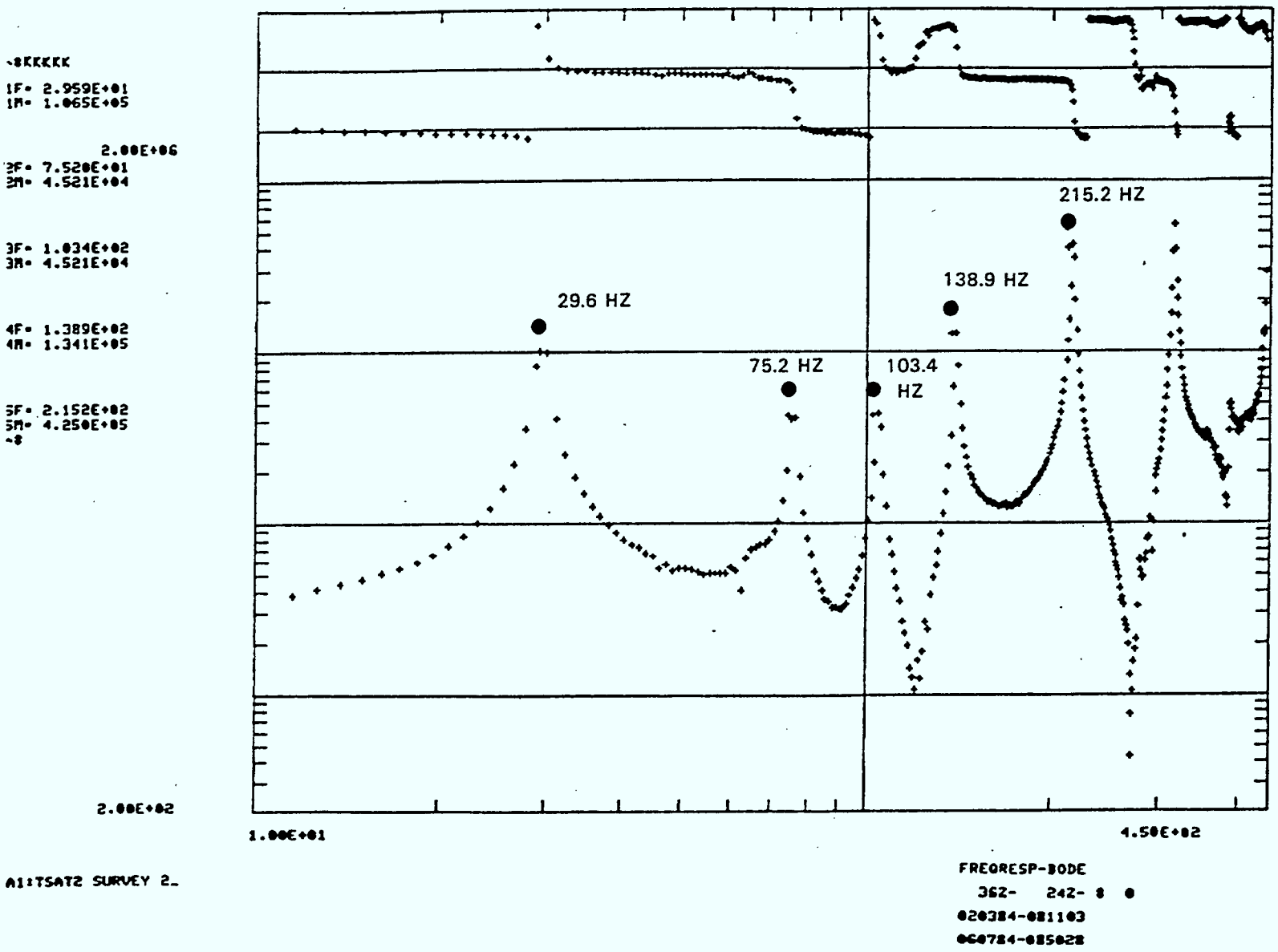

FIGURE 4-3 SECONDARY STRUCTURE EXPERIMENTAL FRF

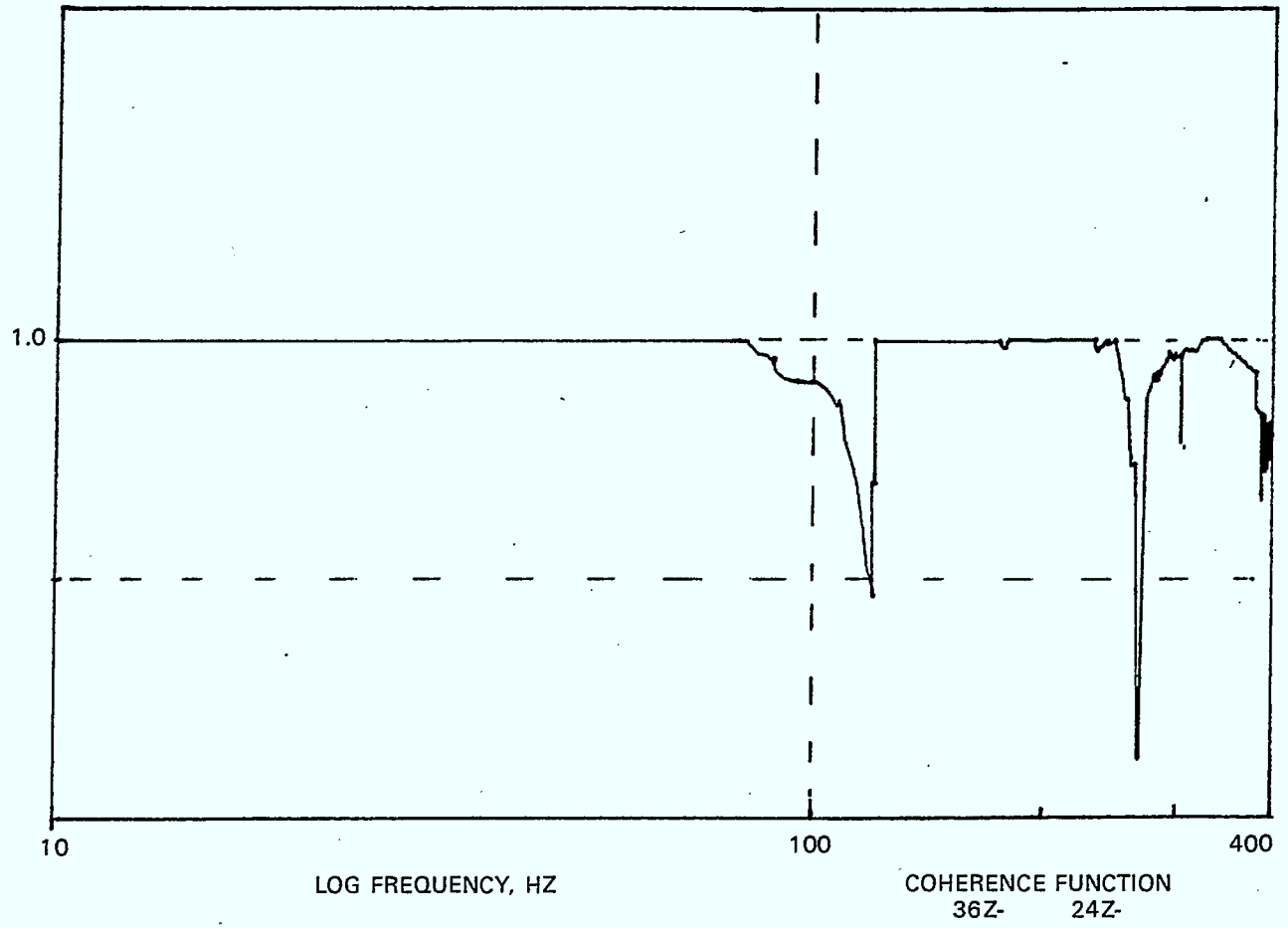

FIGURE 4-4 SECONDARY STRUCTURE COHERENCE FUNCTION

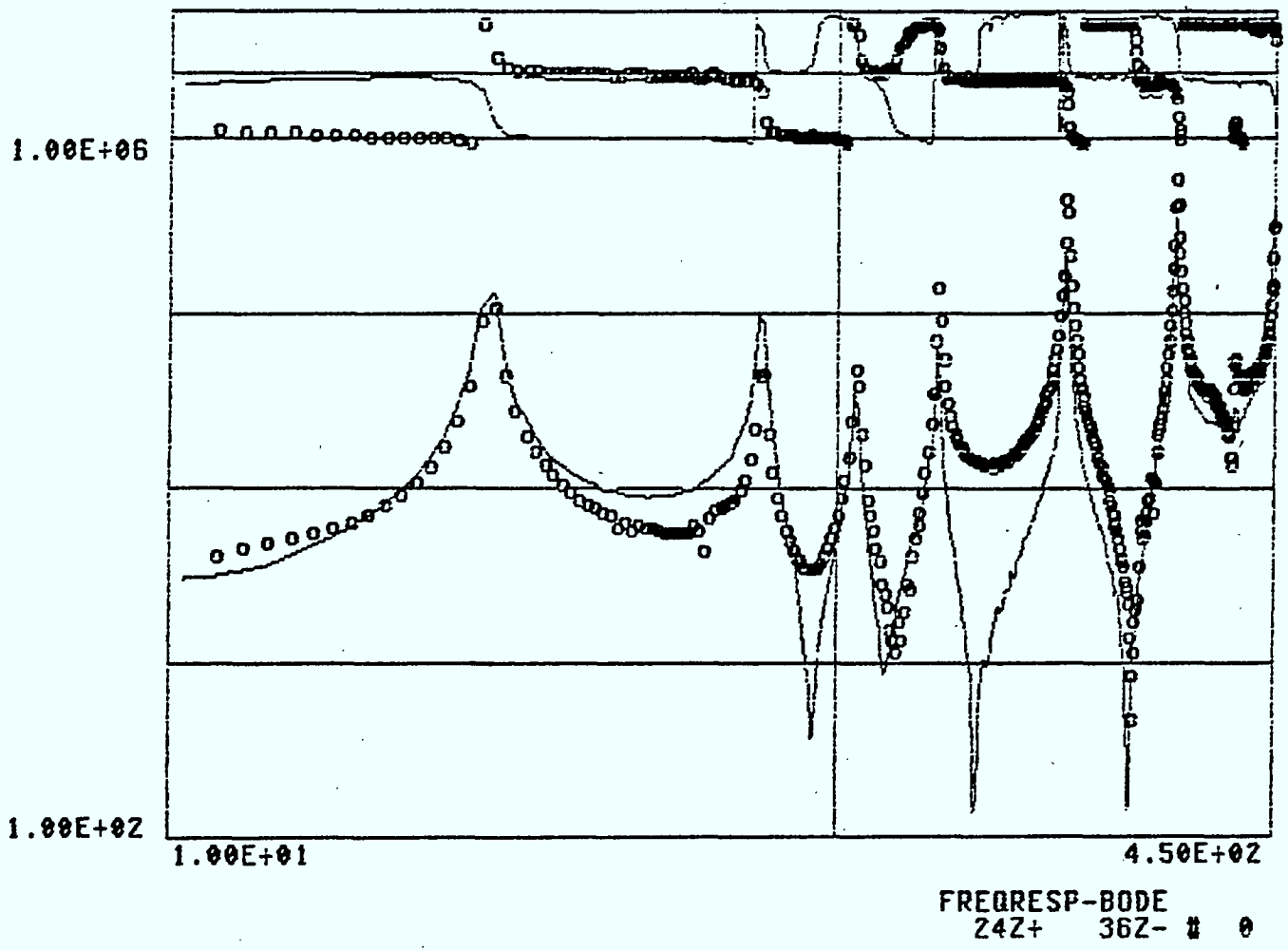

RECIPROCITY
CHECK

FIGURE 4-5 T-SAT SECONDARY STRUCTURE FRF

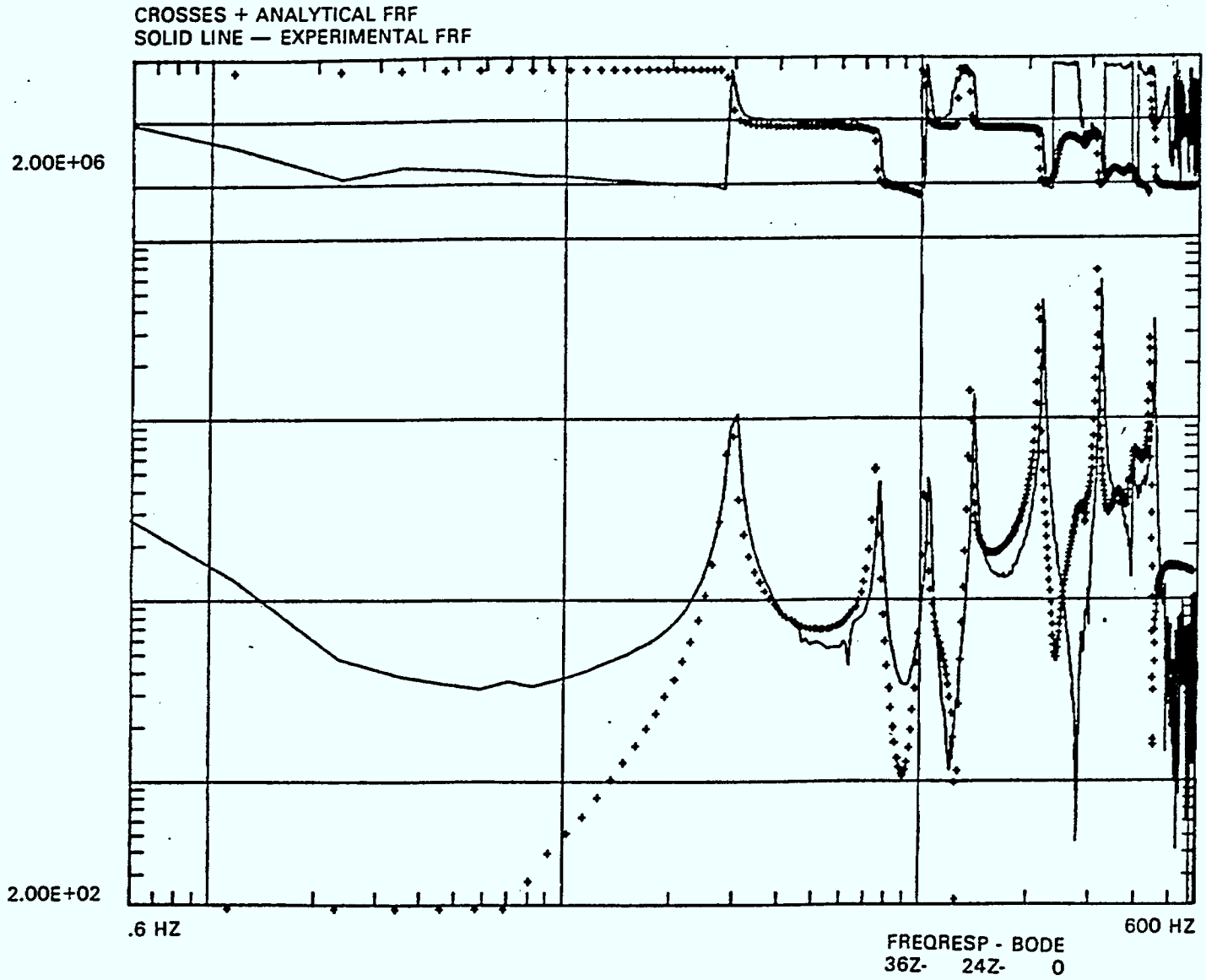

FIGURE 4-6 SECONDARY STRUCTURE CURVE FIT

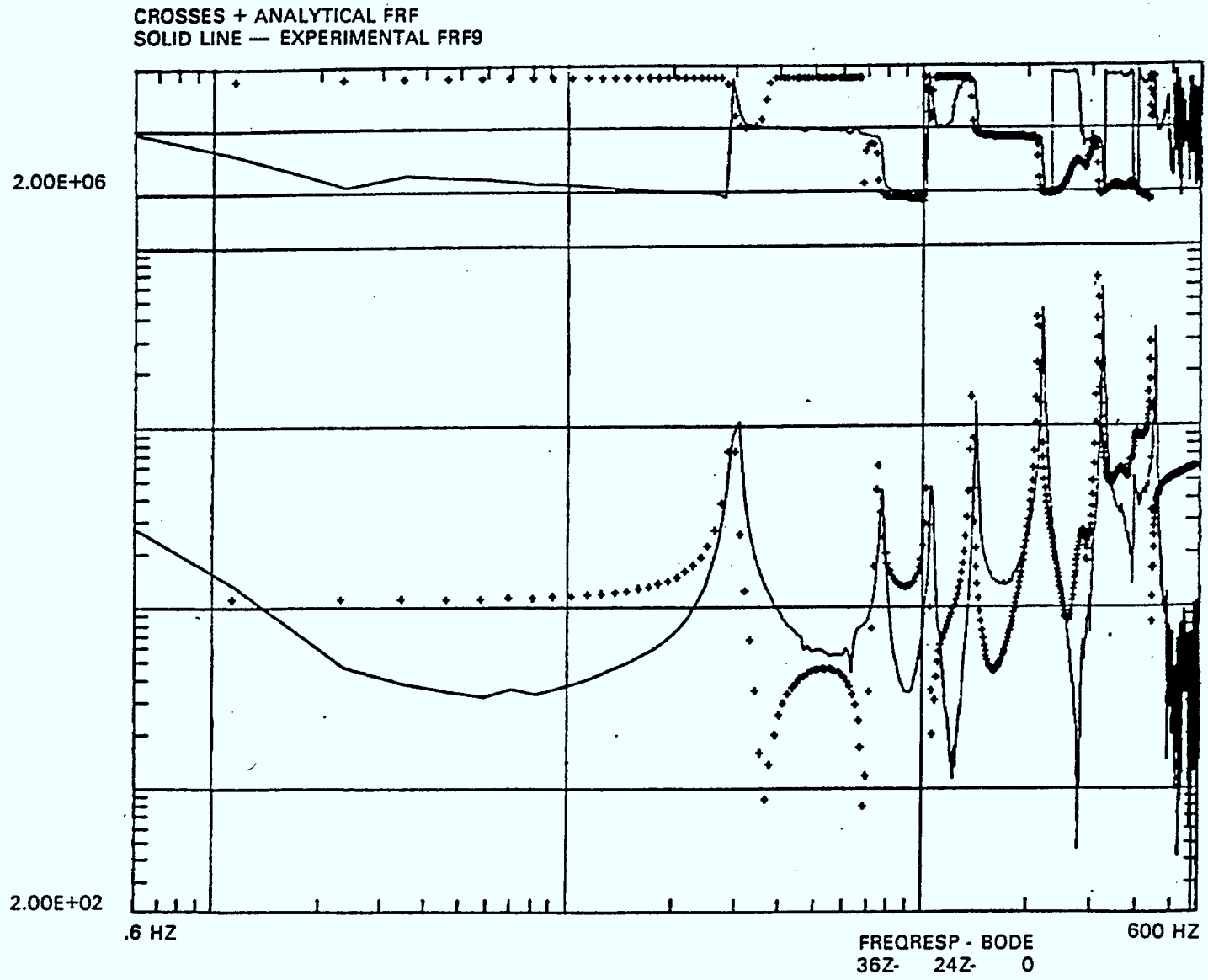

FIGURE 4-7 SECONDARY STRUCTURE CURVE FIT - RESIDUALS ADDED

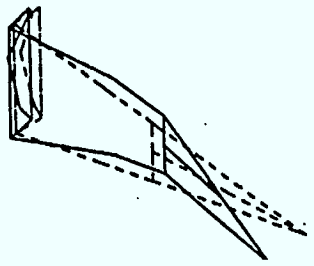

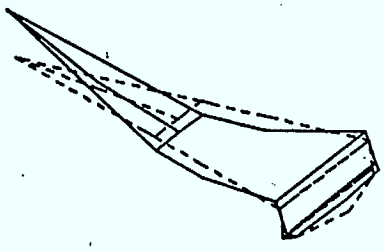

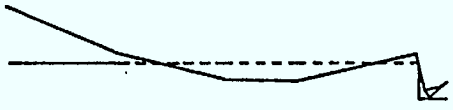

SECONDARY STRUCTURE
1ST BENDING MODE
30.0 HZ.

FIGURE 4-8

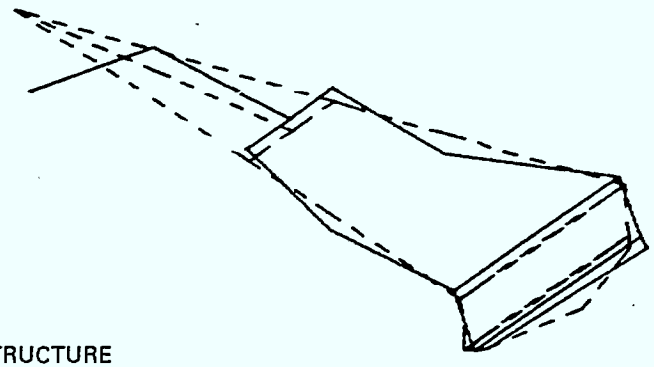

SECONDARY STRUCTURE
2ND BENDING MODE
76.8 HZ.

FIGURE 4-9

	1	2	3	4	5	6	7	8	9	10	11	12	13	14	15	16	17	18
1	1	.18	.01	.28	.19	.02												
2		1	0	.19	0	.02												
3			1	0	0	.12												
4				1	0	.01	.16	.02	.63									
5					1	.05	.05	.39	.02									
6						1	0	.65	0									
7							1	.03	.35	0	.07	.07						
8								1	.06	.02	.01	.31						
9									1	0	.75	.04						
10										1	0	0	.02	.03	.07			
11											1	.01	.58	.07	.01			
12												1	.02	.51	.03			
13													1	.01	.11	.23	.11	.16
14														1	.02	.27	0	0
15															1	.10	0	.03
16																1	.01	.01
17																	1	.89
18																		1

LINEAR RELATIONSHIPS?

MODE 6 AND 8 (213 HZ; 224 HZ)
MODE 4 AND 9 (140 HZ; 293 HZ)
MODE 9 AND 11 (293 HZ; 319 HZ)
MODE 11 AND 13 (319 HZ; 361 HZ)
} NOT SAME MODE

MODE 17 AND 18 (449 HZ; 449 HZ) YES

FIGURE 4-10 MODAL ASSURANCE CRITERIA SECONDARY STRUCTURE

ROOT	FREQUENCY	DAMPING	AMPLITUDE	PHASE
1	0.983	1.00000	2.80187E+05	0.000
2	2.509	1.00000	12006.	3.142
3	29.977	0.01822	3.84557E+05	-1.571
4	36.755	0.97086	29620.	-1.571
5	73.691	0.11261	56392.	1.571
6	76.837	0.00875	3.14004E+05	1.571
7	105.928	0.00755	2.44021E+05	-1.571
8	140.813	0.00520	7.37776E+05	-1.571
9	141.668	0.05063	67577.	1.571
10	162.343	0.15787	2.72796E+06	1.571
11	213.699	0.00450	74803.	-1.571
12	218.466	0.00441	2.79694E+06	1.571
13	223.891	0.06135	4.12437E+05	1.571
14	279.389	0.34248	1.02597E+07	1.571
15	292.722	0.05723	2.85504E+06	1.571
16	297.228	0.00856	1.73497E+05	-1.571
17	318.949	0.00333	4.98740E+06	1.571
18	319.876	0.01058	1.08897E+06	-1.571
19	360.920	0.06613	4.54509E+06	1.571
20	376.304	0.03690	54229.	1.571
21	389.328	0.36153	4.51923E+07	-1.571
22	391.822	0.00896	3.51699E+05	1.571
23	405.188	0.02202	2.26151E+06	1.571
24	449.074	0.00343	5.73329E+05	1.571
25	449.341	0.00316	3.21691E+06	-1.571
26	496.737	0.00020	2.15359E+05	1.571
27	506.833	0.00630	1.82722E+05	1.571
28	522.614	0.00256	2071.2	1.571
29	540.054	0.01444	33016.	-1.571
30	554.428	0.16791	8.02863E+06	1.571
31	585.724	0.00114	993.74	1.571
32	600.169	0.01922	1.09160E+06	0.000
33	663.309	0.42617	1.11674E+07	3.142

4-1 SECONDARY STRUCTURE ESTIMATED ROOTS

```
P
ODAL PARAMETERS, 1
ABEL    FREQ     DAMPING AMPLITUDE   PHASE    REF     RES    MODE    FLAGS
 1     29.977   0.01822 4.4359E+05   1.571   36Z-    36Z-     3    0 0 1 1 1
 2     76.837   0.00875 3.7457E+05   1.571   36Z-    36Z-     6    0 0 1 1 1
 3    105.928   0.00755 1.1925E+04  -1.571   36Z-    36Z-     7    0 0 1 1 1
 4    140.813   0.00520 1.3534E+06   1.571   36Z-    36Z-     8    0 0 1 1 1
 5    141.668   0.05063 3.3982E+04  -1.571   36Z-    36Z-     9    0 0 1 1 1
 6    213.699   0.00450  9009.      -1.571   36Z-    36Z-    11    0 0 1 1 1
 7    218.466   0.00441 1.3979E+06   1.571   36Z-    36Z-    12    0 0 1 1 1
 8    223.891   0.06135 6.7805E+04  -1.571   36Z-    36Z-    13    0 0 1 1 1
 9    292.722   0.05723 7.9786E+05  -1.571   36Z-    36Z-    15    0 0 1 1 1
10    297.228   0.00856 2.2542E+04   1.571   36Z-    36Z-    16    0 0 1 1 1
11    318.949   0.00333 2.1123E+05   1.571   36Z-    36Z-    17    0 0 1 1 1
12    319.876   0.01058 1.9951E+06   1.571   36Z-    36Z-    18    0 0 1 1 1
13    360.920   0.06613 1.7199E+06  -1.571   36Z-    36Z-    19    0 0 1 1 1
14    376.304   0.03690 2.0899E+04   1.571   36Z-    36Z-    20    0 0 1 1 1
15    391.822   0.00896  8082.      -1.571   36Z-    36Z-    22    0 0 1 1 1
16    405.188   0.02202 1.1683E+04   1.571   36Z-    36Z-    23    0 0 1 1 1
17    449.074   0.00343 1.5395E+06  -1.571   36Z-    36Z-    24    0 0 1 1 1
18    449.341   0.00316 4.0696E+06   1.571   36Z-    36Z-    25    0 0 1 1 1
```


TABLE 4-2 SECONDARY STRUCTURE MODAL PARAMETERS

TABLE 4-3

SECONDARY STRUCTURE RESULTS

FREQUENCY (HZ)	DAMPING (%)	MODE	DESCRIPTION OF MODE	NORMALIZED MODAL MASS
30.0	2	1	1ST BENDING	5.3×10^{-4}
76.8	1	2	2ND BENDING	4.9×10^{-4}
105.9	1	3	1ST TORSION	1.4×10^{-3}
140.8	1	4	BENDING	3.5×10^{-4}
141.7	5	5	BENDING	3.5×10^{-1}
213.7	0.4	6	TORSION	1.1×10^{-2}
218.5	0.4	7	BENDING	4.7×10^{-4}
223.9	6	8	TORSION (SUSPICIOUS MODE)	4.0×10^{-2}
292.7	6	9	BENDING (SUSPICIOUS MODE)	7.6×10^{-4}
297.2	1	10	TORSION	3.5×10^{-2}

TABLE 4-3 - Continued

FREQUENCY (HZ)	DAMPING (%)	MODE	DESCRIPTION OF MODE	NORMALIZED MODAL MASS
318.9	0.3	11	BENDING	5.9×10^{-5}
319.9	1	12	BENDING	4.8×10^{-2}
360.9	7	13	TORSION (SUSPICIOUS MODE)	2.7×10^{-3}
376.3	4	14	TORSION - FLANGE MOTION	1.5×10^{-2}
391.8	1	15	TORSION	4.7×10^{-4}
405.2	2	16	TORSIONAL BENDING	1.3×10^{-4}
449.1	0.3	17	BENDING	1.4×10^{-3}

5.0 PRIMARY STRUCTURE TESTS

The primary structure was tested in a fixed-free configuration with several types of excitation input. Sections 5.2 and 5.3 describe the results of the base and portable shaker excitation. Section 5.4 compares and discusses the results. The accelerometer locations and coordinate locations were common for all tests of the primary structure.

To facilitate description of the bending modes of the structure shelf, the nomenclature illustrated in Figure 5-1 will be used.

5.1 TEST CONFIGURATION

Figure 5-2 shows the instrument configuration for the primary structure and Figure 5-3 shows the corresponding geometric coordinates. The following is a list of the coordinates (in inches).

Figure 5-1 shows the accelerometer degrees of freedom. Figure 5-2 shows the geometry coordinates. The following is a list of the coordinates (in inches)

	R	0°	Z
2	8.5	0	8.8
3	8.5	90	8.8
4	8.5	180	8.8
5	8.5	270	8.8
6	0	0	21.238
7	9.0	0	21.238
8	9.0	45	21.238
9	9.0	90	21.238
10	9.0	180	21.238
11	9.0	270	21.238
12	8.5	45	8.8
13	18.0	0	21.238
14	18.0	45	21.238
15	18.0	90	21.238
16	18.0	135	21.238
17	18.0	225	21.238
18	18.0	270	21.238
19	18.0	315	21.238
20	18.25	156.6	21.238
21	18.25	180	21.238
22	18.25	203.4	21.238

40	13.25	0	21.238
41	13.25	90	21.238
42	13.25	180	21.238
43	13.25	270	21.238

There were 60 accelerometers used in instrumenting the structure. The structure was mounted to a reaction mass, via the 40,000 lb. electrodynamic shaker table. The shaker was used for the base excitation tests, but it was left in a locked position for the portable shaker test.

5.2 BASE EXCITATION

There were two types of base excitation applied to the primary structure - sine sweep and random. The 40,000 lb. electrodynamic shaker was used for the input. The random test was done for two axes, X and Z (lateral and vertical). The sine sweep was only done for the Z (vertical axis). Section 5.2.3 compares the results.

Table 5-1 lists the base excitation test parameters.

In order to properly process base excitation results, the rigid body motion of the input must be removed from the accelerometer responses. Reference 4 describes the method of processing base results for modal tests.

If the rigid body motion is not removed from the accelerometer response, the frequency response function appears similar at the resonant peaks, but very different elsewhere. Figure 5-4 shows the corrected and uncorrected data. The parameters estimated using either corrected or uncorrected functions are very similar. Figures 5-5 and 5-6 show the overlays of the curves generated from the estimated parameters with the actual experimental data. Though the parameters are the same, a judgement of the quality of fit would suggest that the uncorrected FRF information produces a poor curve fit.

5.2.1 SINE SWEEP TEST RESULTS - There were two types of base excitation applied to the primary structure - sine sweep and random. Figure 5-7 shows the frequency response function for point 6Z, located in the centre of the shelf. Its principal response looked similar to the response of a drum being hit. For most other modes, point 6Z did not have any significant response.

Figure 5-8 shows the coherence function for point 6Z that has been excited in the Z (vertical) direction. The coherence is one over most of the regions with the exception of the resonant peaks, the high frequency components and at 60 Hz. A coherence function drop at a resonant peak is often the result of

insufficient definition of the response (not enough lines available) rather than a physical problem. The high frequency drop resulted from the anti-resonance in that region.

Table 5-2(a) is a list of the predicted modes and their descriptions for the uncorrected FRF case. The frequency sweep was only to 160 Hz, so there are no modes calculated beyond that.

The sine sweep parameters were calculated twice. Initially they were calculated based on all uncorrected frequency response functions using a complex exponential technique based on one frequency response function. Later they were calculated from the corrected Z component frequency response functions located on the structure shelf (using POLYREFERENCE, for one reference point only).

Table 5-2(b) lists the parameters calculated for the corrected FRF case with a descriptive note on the mode shape. The differences between (a) and (b) are due mainly to the frequency response functions used, not the base correction.

The only notable variations in the data seems to be the damping values between corrected and uncorrected sine sweep data. The corrected values predict higher values, which is the expected trend, but the differences are larger than expected from the correction alone.

Figure 5-9 shows a cross-section view of the plate, vibrating in the drum mode (at 75 Hz).

5.2.2 **RANDOM TEST RESULTS** - Figures 5-10 and 5-11 show the frequency response and coherence functions for point 6Z, located in the centre of the shelf. This is the same point for which the sine sweep FRF was displayed (Section 5.2.1). The functions look very similar over the comparable frequency range. In the 30 Hz frequency range, the random data is not as well defined as the sine data, in part because the frequency resolution is finer for the sine sweep data. Further processing of the random data, with improved resolution still indicates that the sine data is better defined.

Figure 5-12 and 5-13 show the frequency response and coherence functions for point 21 X excited in the X (lateral) direction with random input. Point 21 X is located on the external edge of the structure shelf. The coherence function is close to one through most of the region except at the anti-resonances and around 25-30 Hz where some of the primary vertical modes are.

The frequency response function data contains more noise than the Z-axis test.

Table 5-3 lists the frequency, damping and mode shape descriptions. The data from the X-axis test was not processed below 60 Hz because the modes were all Z-axis responses and the Z-axis test was better able to excite them.

5.2.3 COMPARISON OF RANDOM AND SINE SWEEP RESULTS - Table 5-4 lists the frequency and damping results of the sine sweep and random tests.

The random test was not able to excite the modes below 30 Hz well enough to accurately determine the parameters. In part this was due to the lack of frequency resolution, but the sine sweep did seem to do a better job of exciting the anti- and semi-symmetric plate modes.

The frequency estimates for modes common to each test were within 1/2% for modes below 100 Hz and within 5% for those above 100 Hz. The damping values showed a much larger spread, as high as 100%.

There were two modes predicted from the uncorrected sine sweep data (26.227 Hz and 27.627 Hz) which indicated damping significantly higher than the rest of the shelf bending modes. The 26.227 Hz mode is quite possibly just a 'numerical mode' generated by the POLYREFERENCE processing. The 6% damping indicated for the mode at 27.627 Hz may have occurred as POLYREFERENCE tried to predict parameters from an uncorrected curve fit.

The mode shape predicted at 85.5 Hz from the random test data was best excited by the lateral (X-axis) base excitation as it was a lateral/torsion mode. It was not even predicted from the Z-axis sine data, which would suggest that the 'purer' excitation provides less opportunity for cross-coupling.

5.3 PORTABLE SHAKER EXCITATION

The mini-shaker testing was done twice, each time for several excitation points. Though the retest was much more successful, the results of the first test series are included for comparison. POLYREFERENCE processing was used to extract the parameters. Two reference points were used for each set of parameters extracted.

Rather than use all 60 frequency response functions to estimate parameters, the best third for any frequency region were chosen. The frequency and damping values were based on the subset of frequency response functions and then all functions were included for mode shape calculation.

Table 5-5 lists the test parameters for the two portable shaker test series.

5.3.1 FREQUENCY RESPONSE FUNCTIONS - Figures 5-14 and 5-15 are the frequency response and coherence functions taken for one of the driving point locations.

There is significant loss of coherence in the 25-30 Hz range, largely due to the lack of frequency resolution.

Figures 5-16 and 5-17 are the same functions, zoomed over a narrower frequency range (20-50 Hz rather than 10-250 Hz). The zooming has shown up the presence of an additional peak (26.4 Hz) which was in the wider frequency range.

The coherence function has improved, but only slightly. Additional zooming was not possible due to the length of data sample taken.

5.3.2 PARAMETER AND MODE SHAPE ESTIMATION - Figure 5-18 is one of the curve fits done for the mini-shaker data. Table 5-6 lists the parameters used to generate this curve. The first four modes show fairly good fit to the data. The last one, which is actually the drum mode is a very poor fit which will underestimate the damping.

Table 5-7 lists the parameters estimated from each test, along with a description of the mode shapes. The modal masses have not been normalized.

For 'plate' dominated modes, the masses are quite different for the initial and retest results, probably indicating that the change of reference coordinates was significant in terms of how well each mode was excited.

An estimate of the parameters from one frequency response function based on zoomed data indicated that damping was overestimated for three of the four modes. Figure 5-19 shows the zoomed curve fit.

5.3.3 DISCUSSION OF RESULTS - Table 5-8 lists the parameters obtained from mini-shaker test series as well as those based on the zoomed FRF.

The first test series missed the mode whose frequency was in the 27.2 to 27.4 Hz range, and the possible mode at 57.6 Hz. The frequency estimates for common modes are within 1%. The damping values vary by more than 100% in some cases.

Several modes were predicted near 87 Hz. It was not possible to establish how many modes actually existed, though it is likely that there were at least two. The mini-shaker retest did predict more than one mode, but based on modal assurance and curve fit criteria, several were suppressed. Additional testing, positioning the mini-shakers based on the predicted mode shapes for these modes, would have been needed to determine the true modes.

5.4 DISCUSSION OF PRIMARY STRUCTURE RESULTS

Table 5-9 lists the parameters for the test configurations of the primary structure. Both the base and mini-shaker tests were able to predict all dominant modes of the structure.

The first three (shelf) modes were weakly excited by the base test. The mini-shaker test configuration did not result in a strong response for the drum mode. In fact this was an example of an internal mode which would be difficult for a mini-shaker to access.

The results presented in Table 5-4 represent the 'best' combination of results used for each configuration. Results processed using POLYREFERENCE tended to have higher damping values.

Random test results were not processed below 30 Hz. Modes near 85 Hz were very confusing. It is still not clear how many modes exist there - either 1 or 2 is most likely. In processing some modes were predicted by the software but were suppressed. It is possible that the shift in frequency for the drum mode in the base and mini-shaker tests is due to the presence of more than one mode, due to the anisotropic nature of the material. In fact the base tests predicted more than one mode, but it was analytically suppressed.

The sine and random tests were much easier and quicker to perform. The emphasis in processing the results was on the mini-shaker test results because modal mass was needed for the subsequent substructure coupling work.

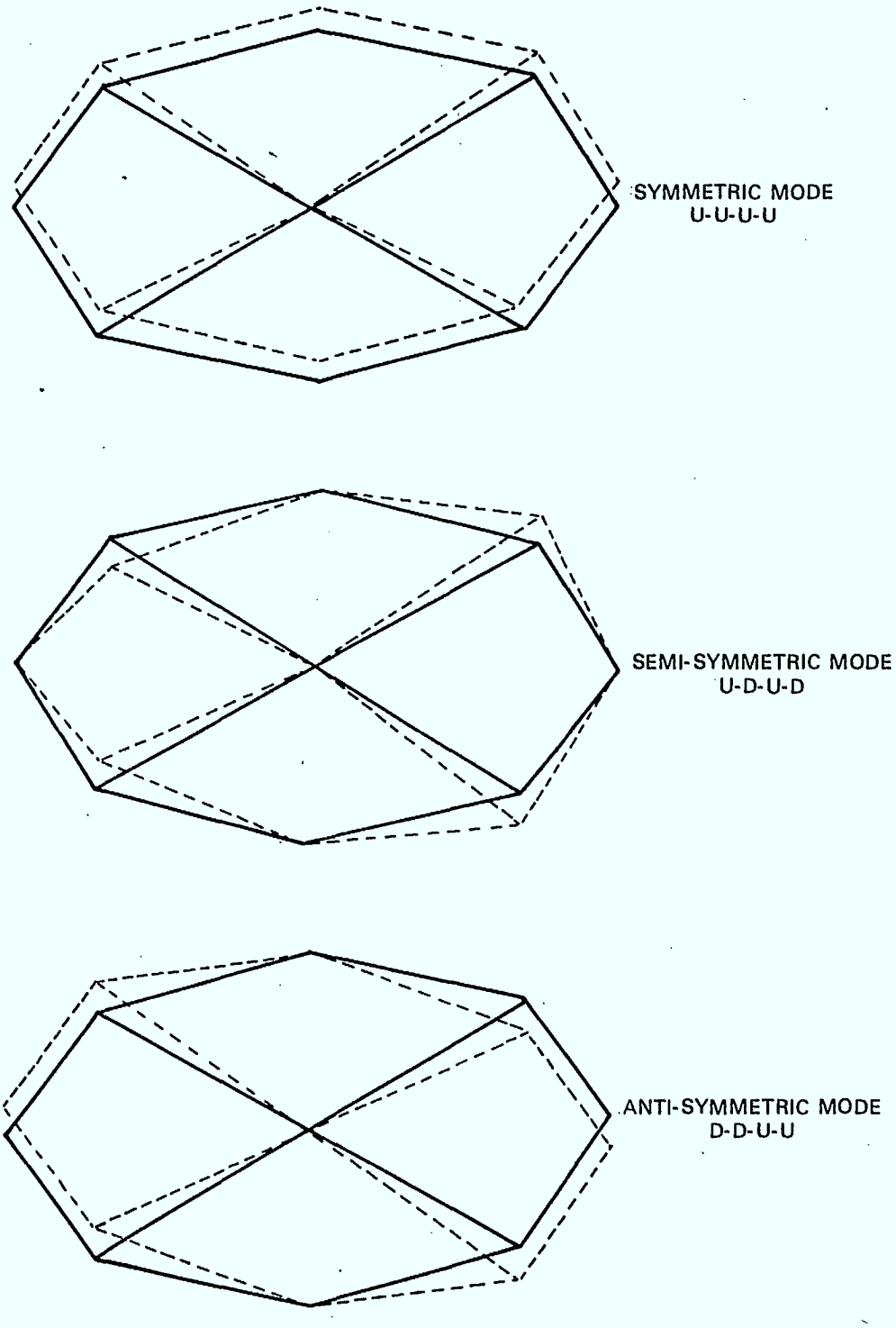

FIGURE 5-1 DESCRIPTION OF PLATE MODES

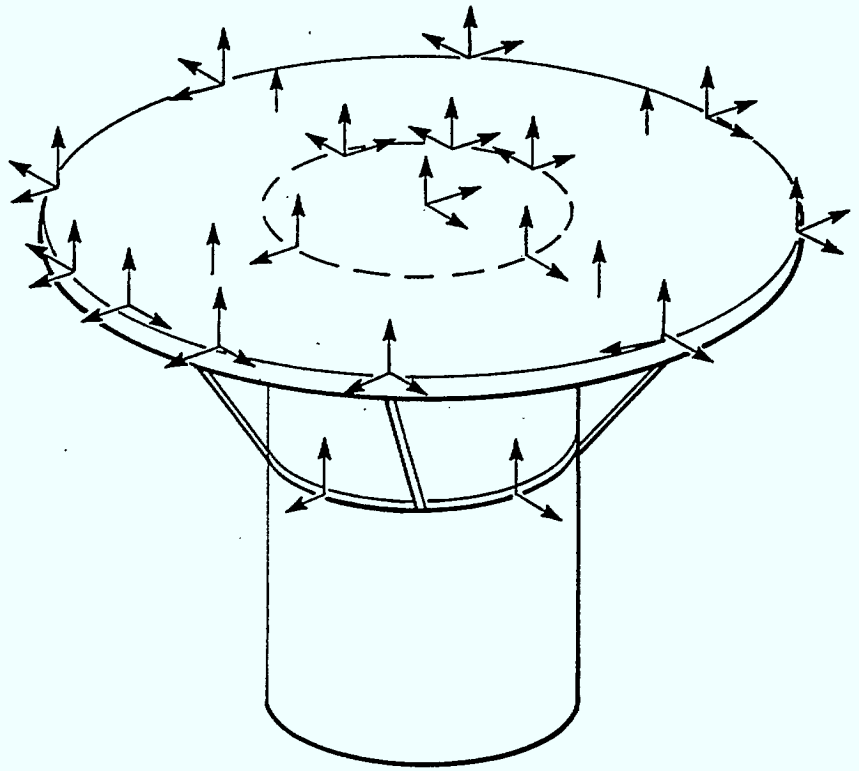

FIGURE 5-2 T-SAT PRIMARY STRUCTURE INSTRUMENT CONFIGURATION

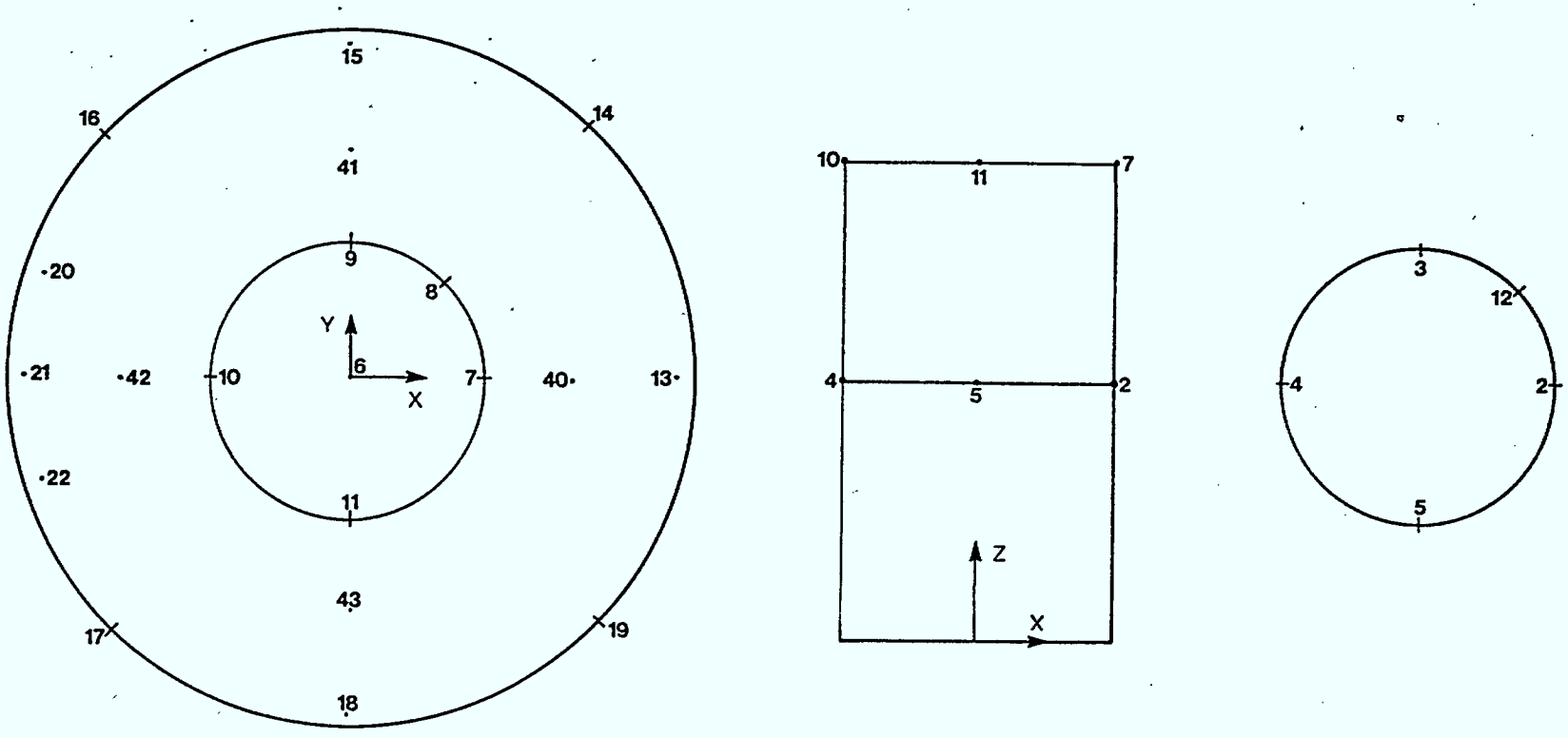

STRUTS CONNECT TO
POINTS 14, 16, 17, 19

FIGURE 5-3 GEOMETRIC COORDINATES

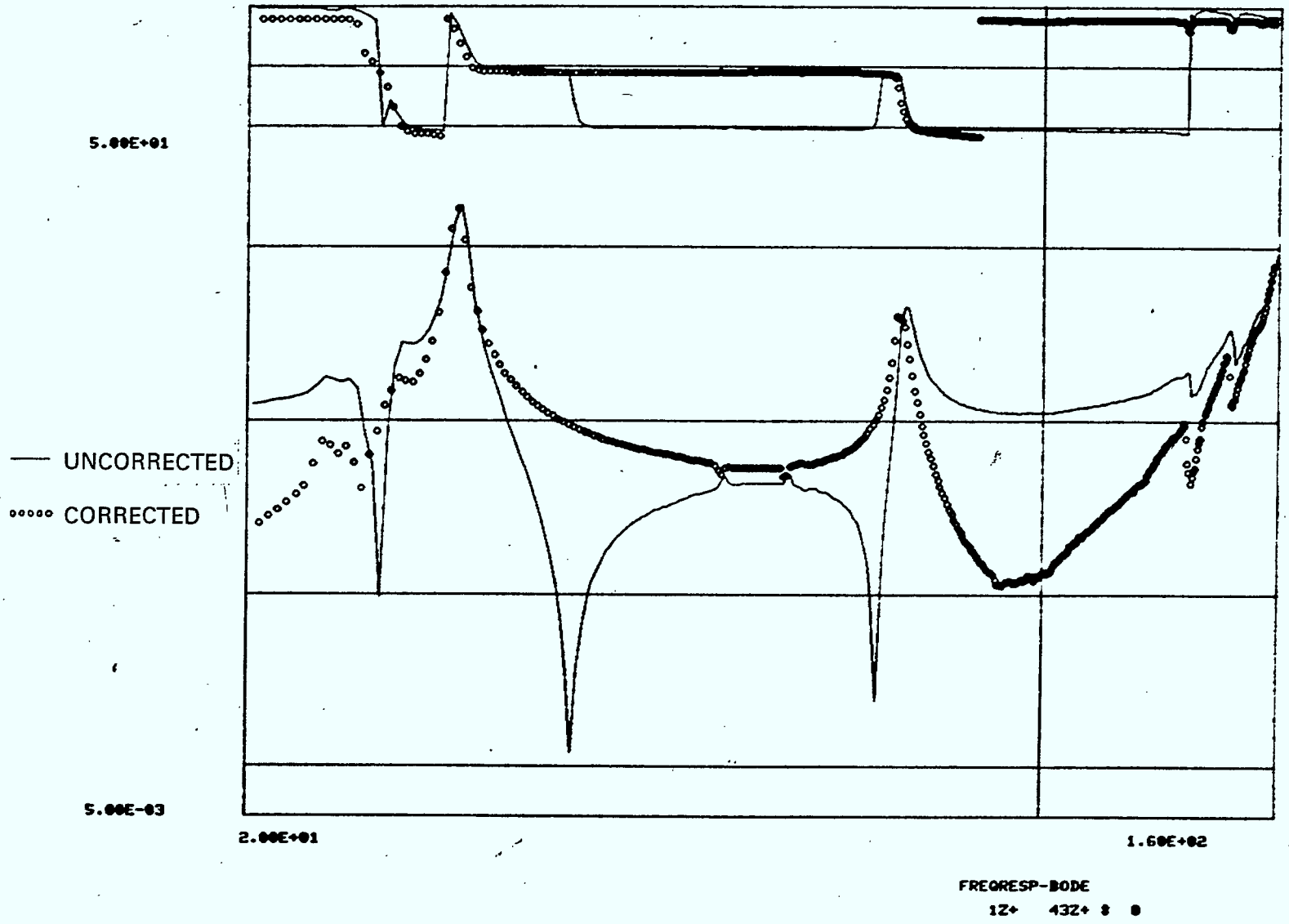

FIGURE 5-4 BASE EXCITATION FRF's

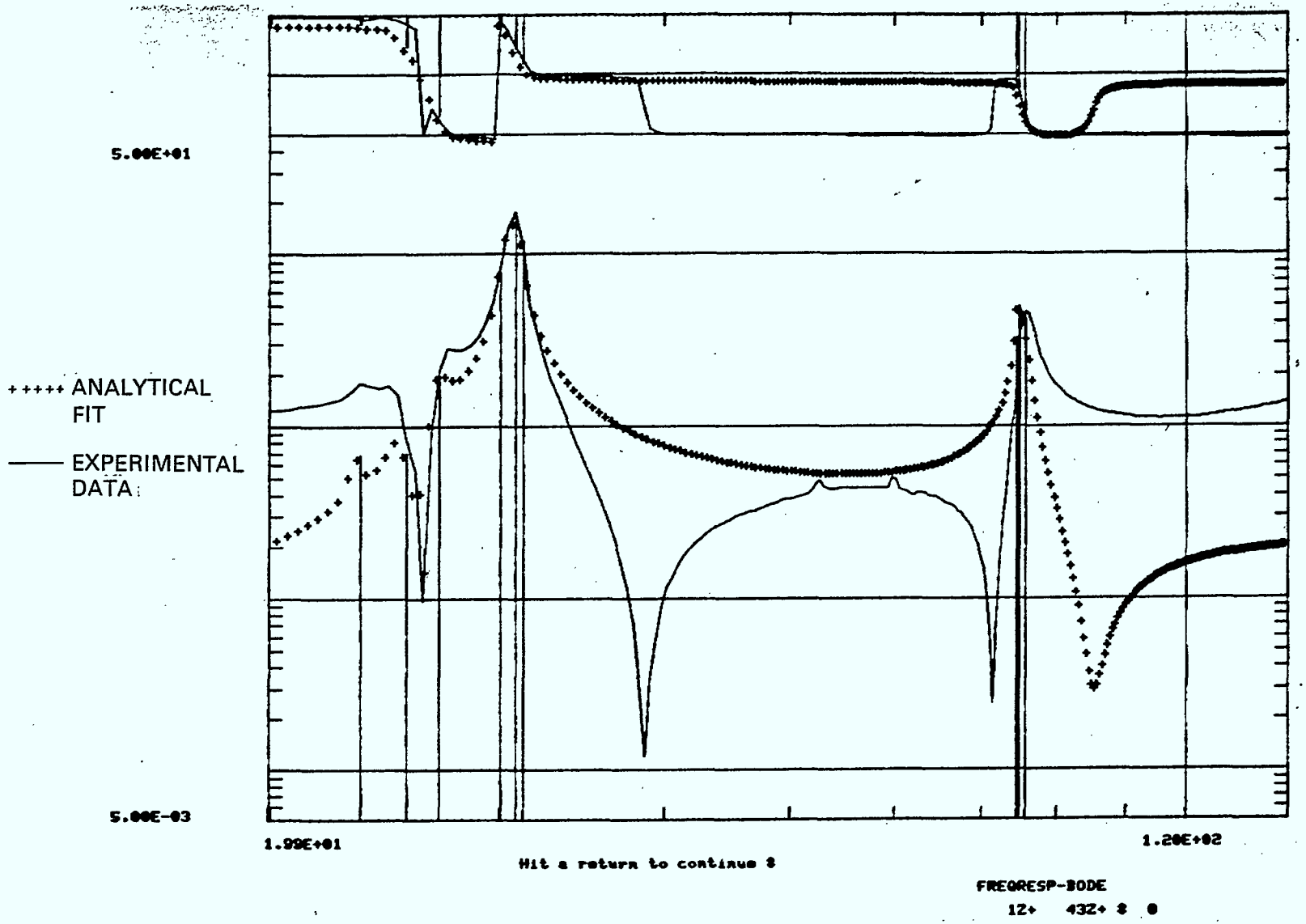

FIGURE 5-5 POLYREFERENCE CURVE FIT - UNCORRECTED BASE

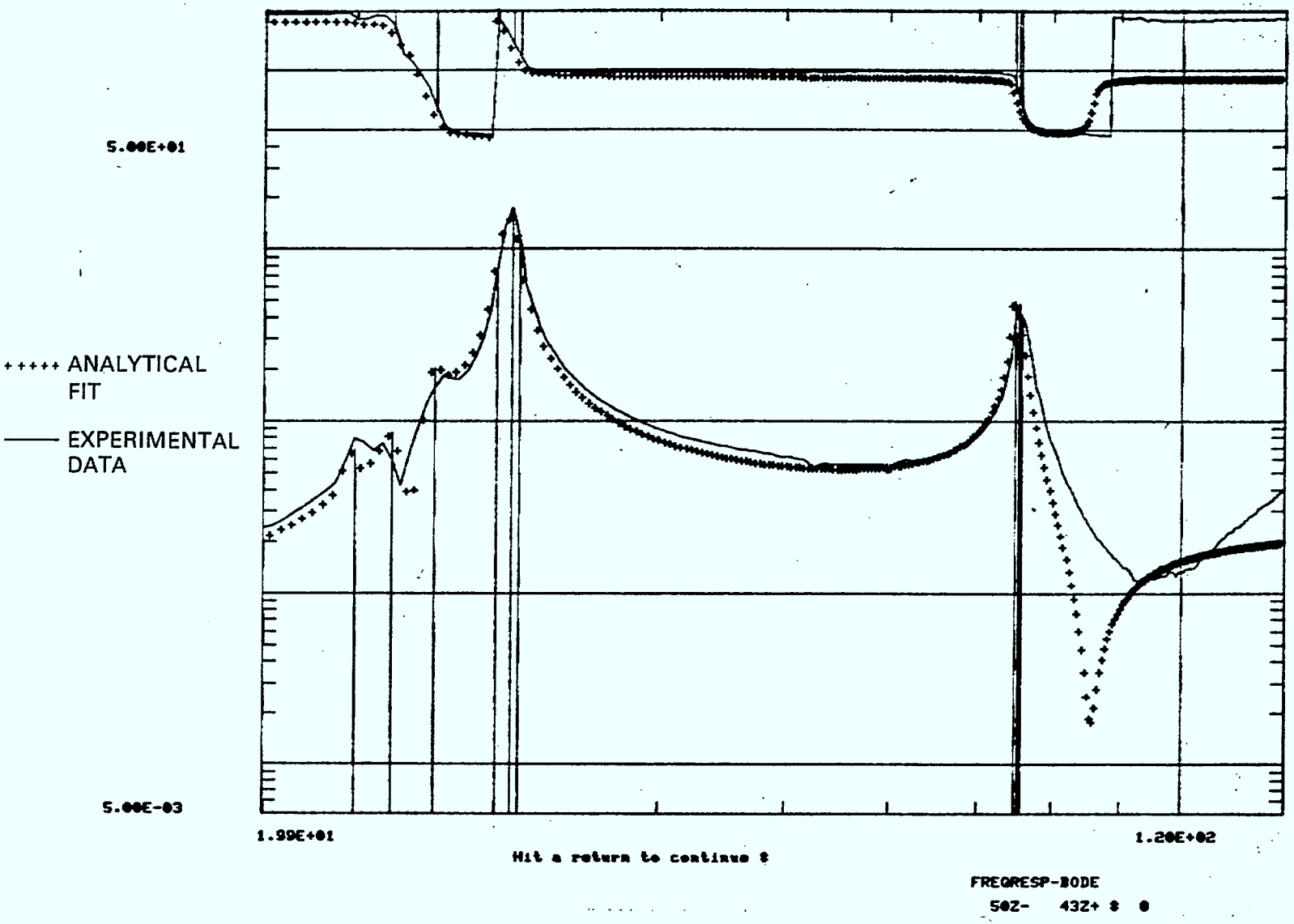

FIGURE 5-6 POLYREFERENCE CURVE FIT - CORRECTED BASE

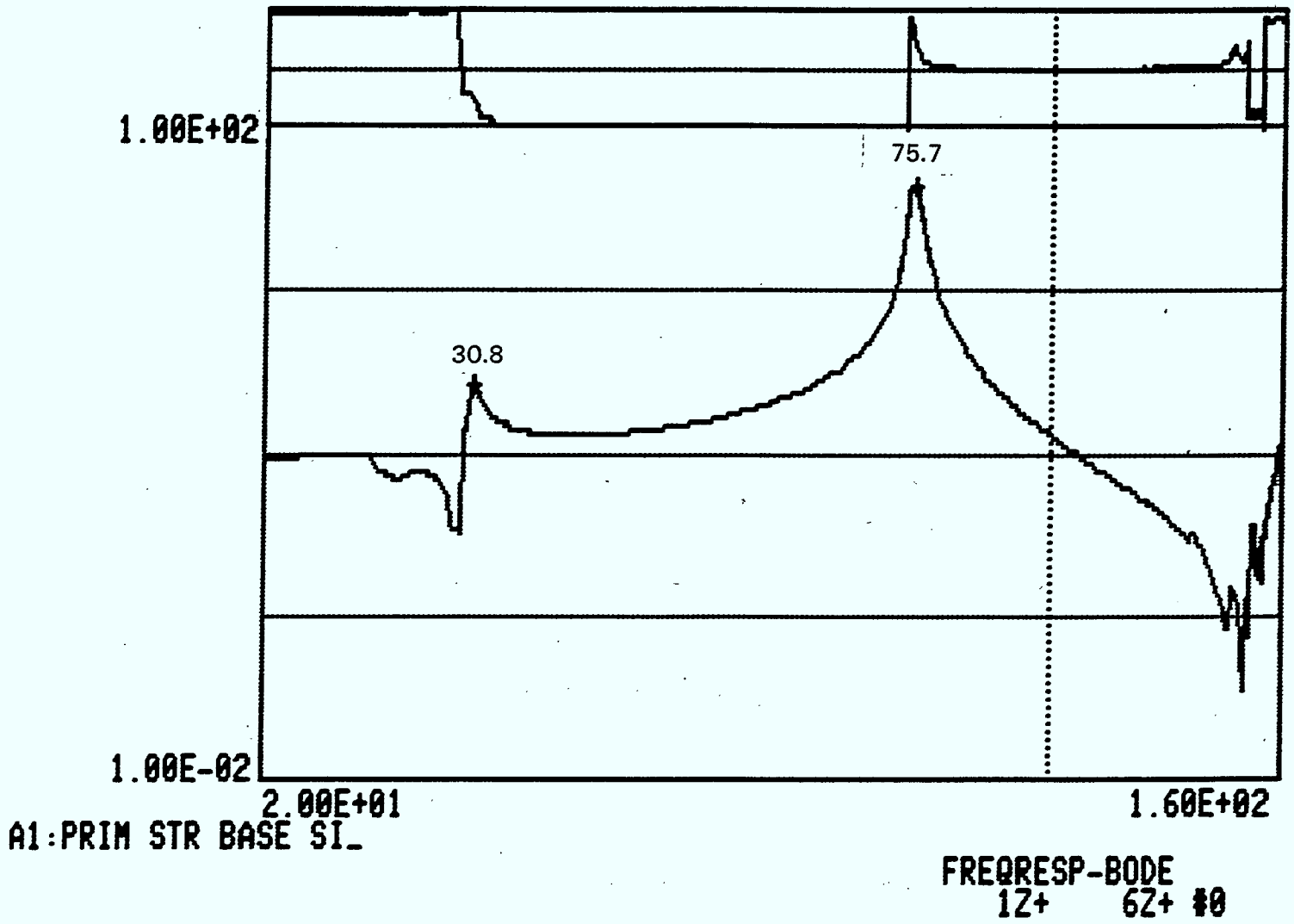

FIGURE 5-7 PRIMARY STRUCTURE EXPERIMENTAL FRF (BASE, SINE EXCITATION)

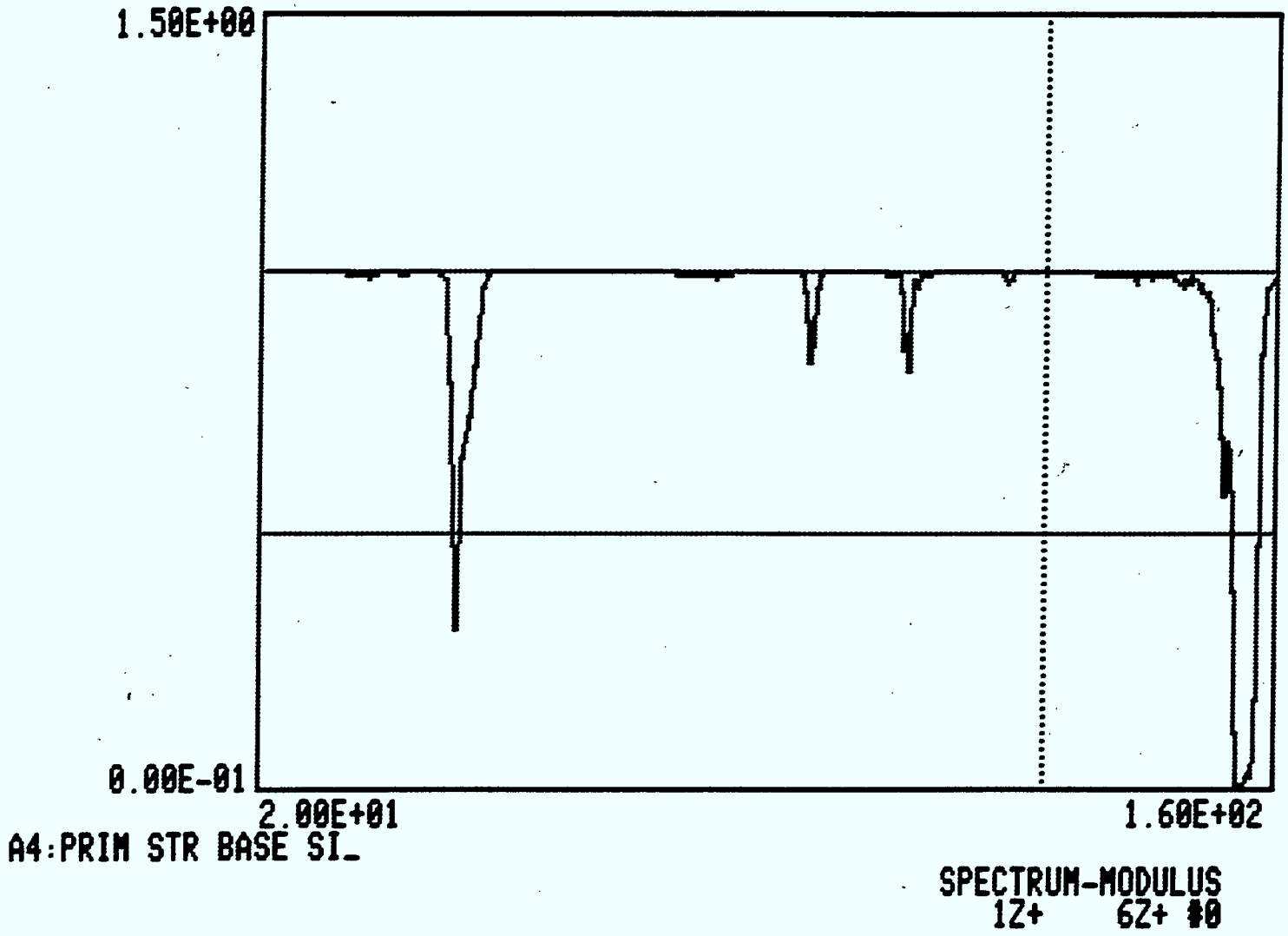

FIGURE 5-8 PRIMARY STRUCTURE COHERENCE FUNCTION (SINE, BASE EXCITATION)

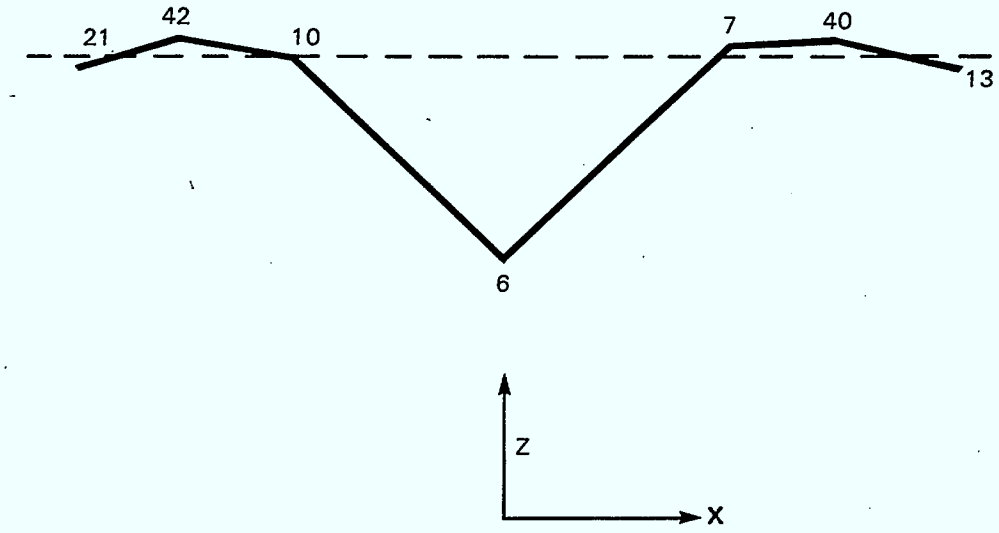

FIGURE 5-9 DRUM MODE

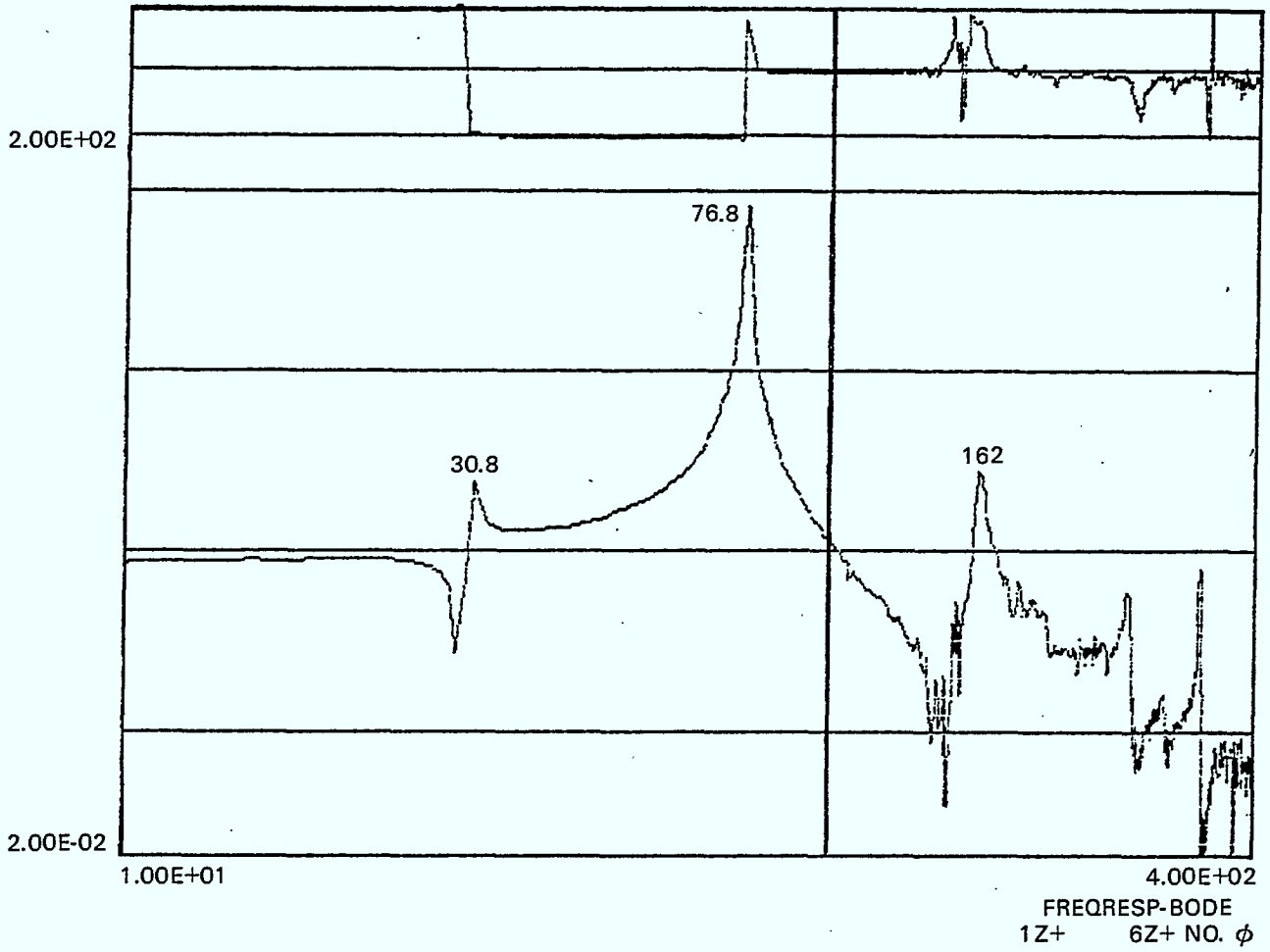

FIGURE 5-10 PRIMARY STRUCTURE EXPERIMENTAL FRF (RANDOM, BASE EXCITATION)

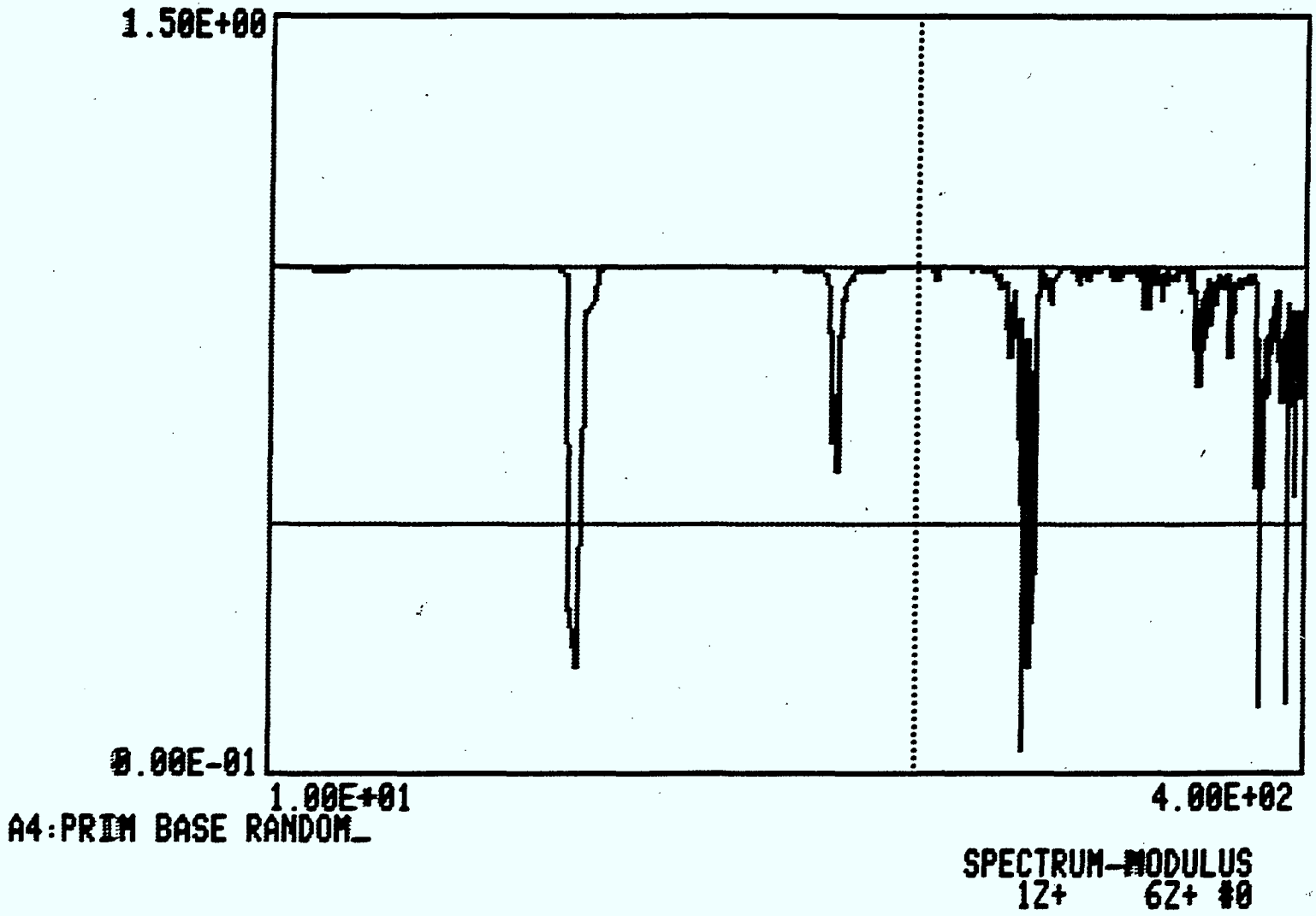

FIGURE 5-11 PRIMARY STRUCTURE COHERENCE FUNCTION (RANDOM, BASE EXCITATION)

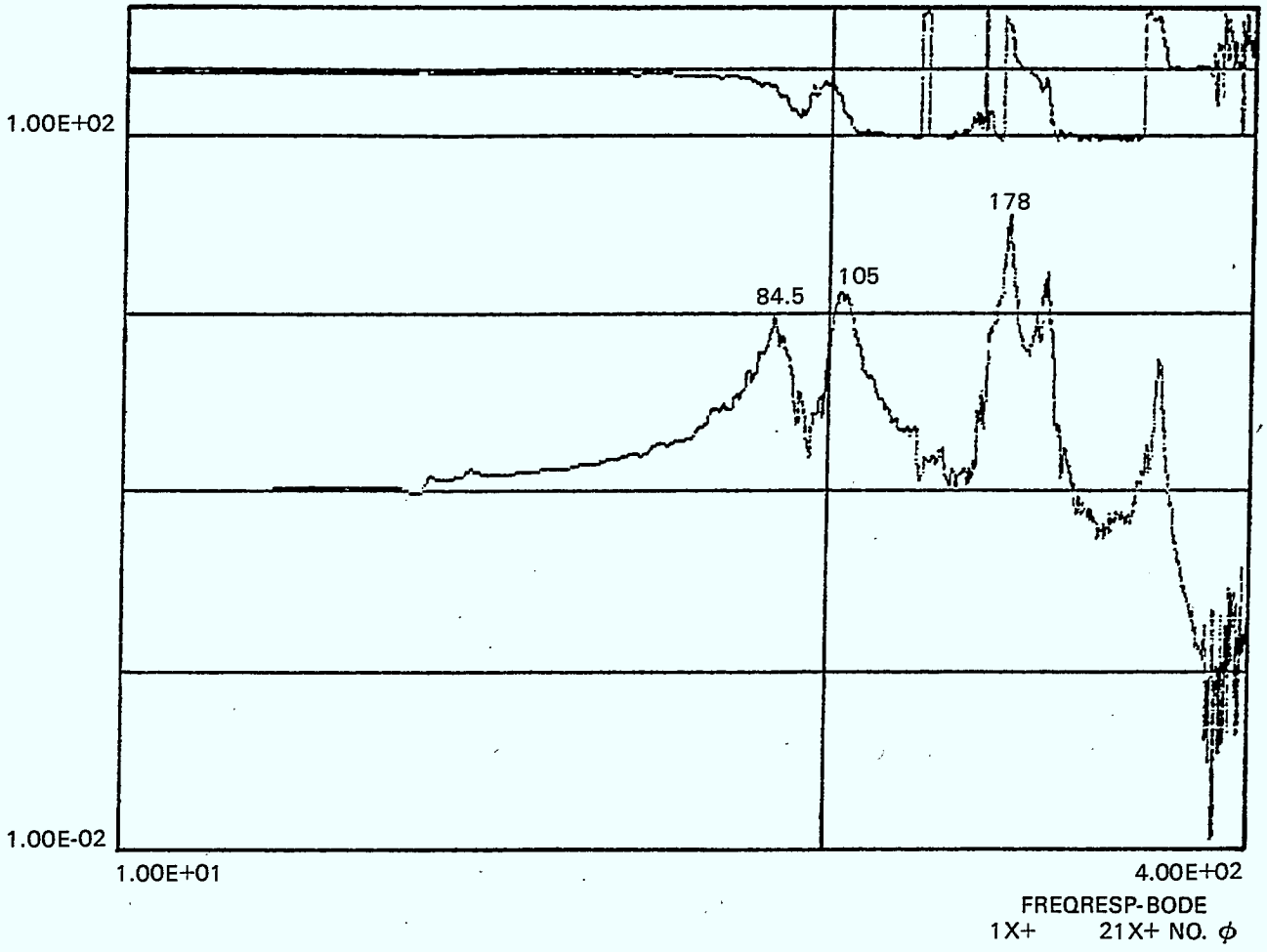

FIGURE 5-12 PRIMARY STRUCTURE EXPERIMENTAL FRF (RANDOM, BASE EXCITATION)

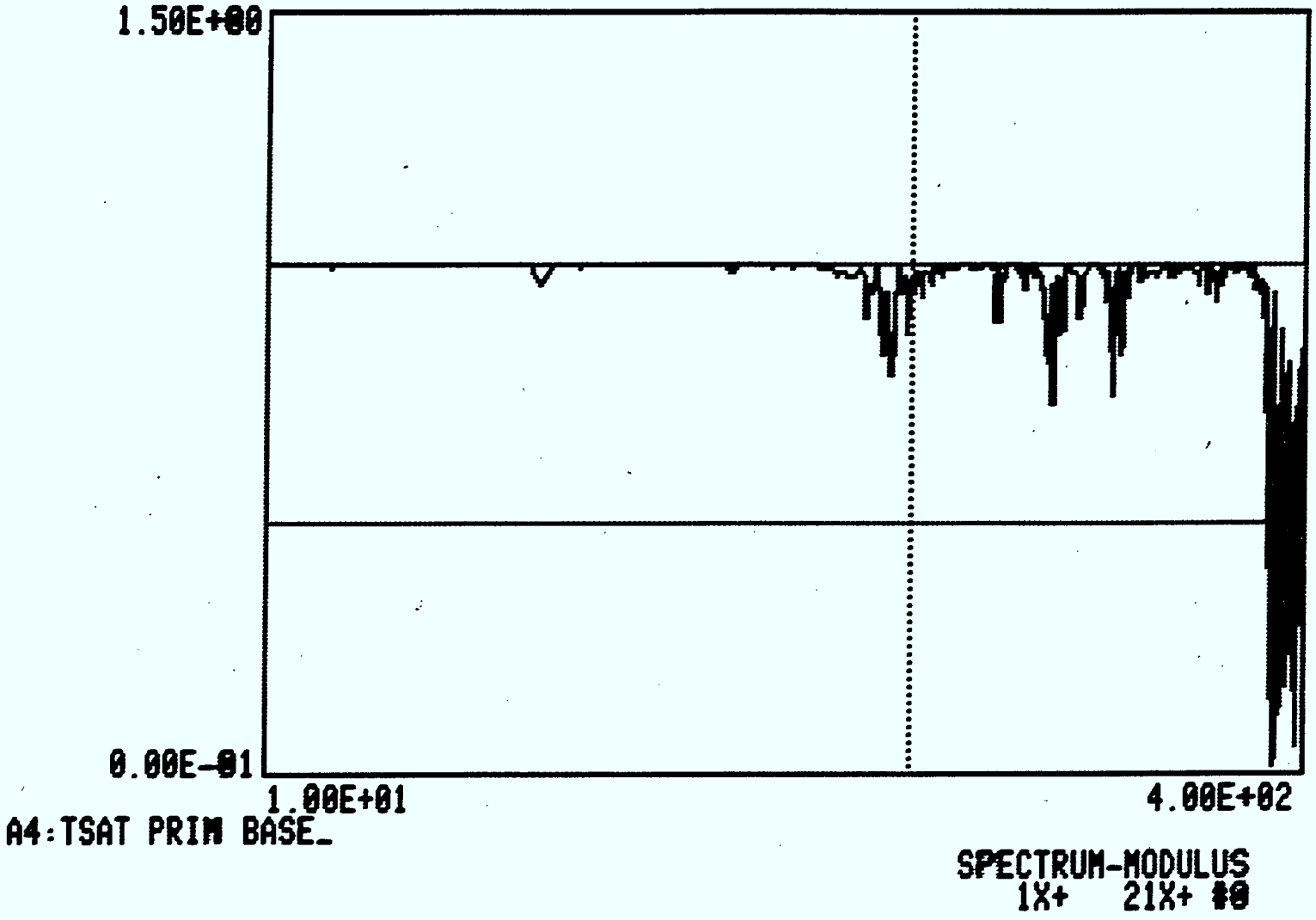

FIGURE 5-13 PRIMARY STRUCTURE COHERENCE FUNCTION (RANDOM, BASE EXCITATION)

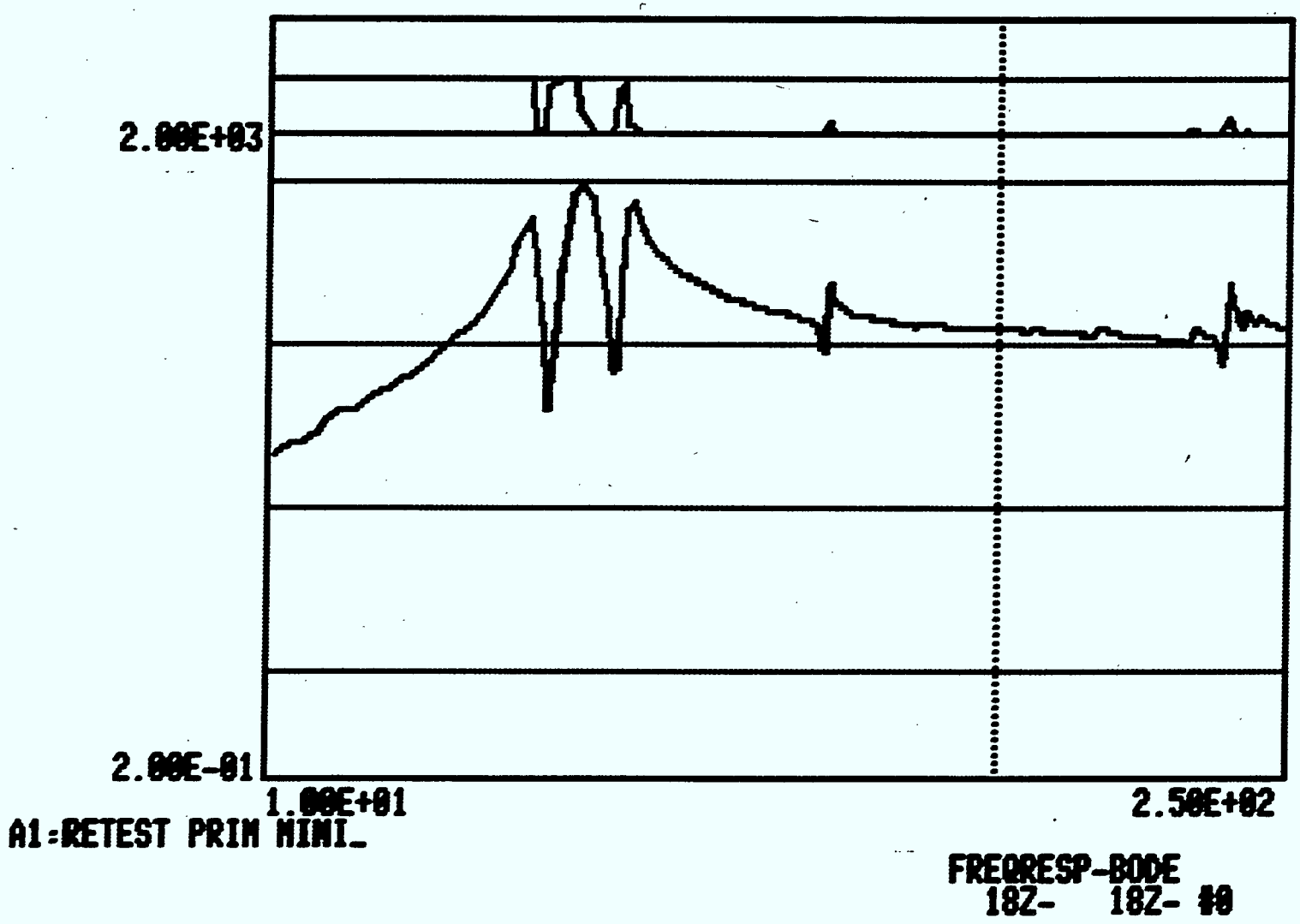

FIGURE 5-14 PRIMARY STRUCTURE EXPERIMENTAL FRF (MINI SHAKER, RETEST)

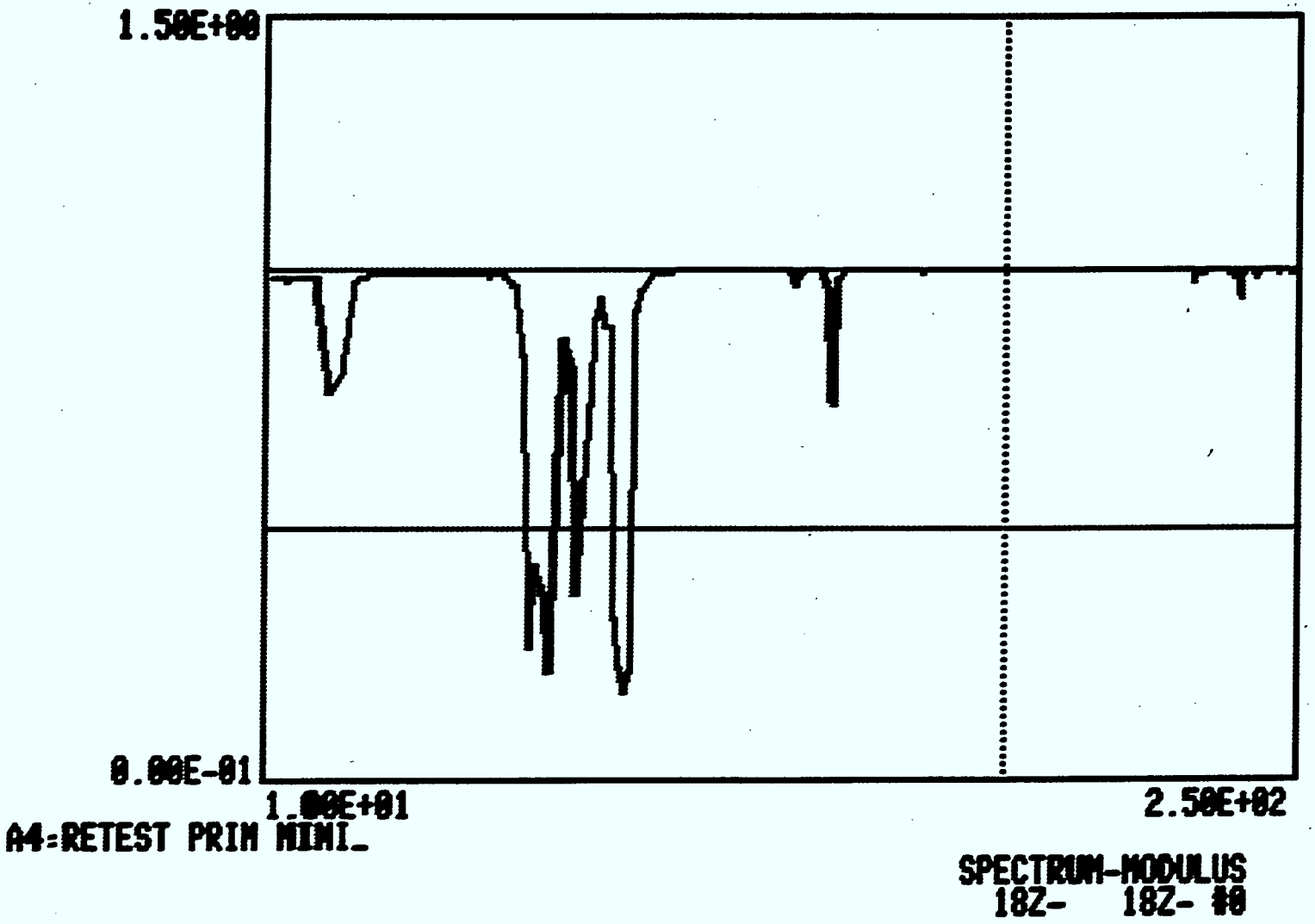

FIGURE 5-15 PRIMARY STRUCTURE COHERENCE FUNCTION (MINI SHAKER, RETEST)

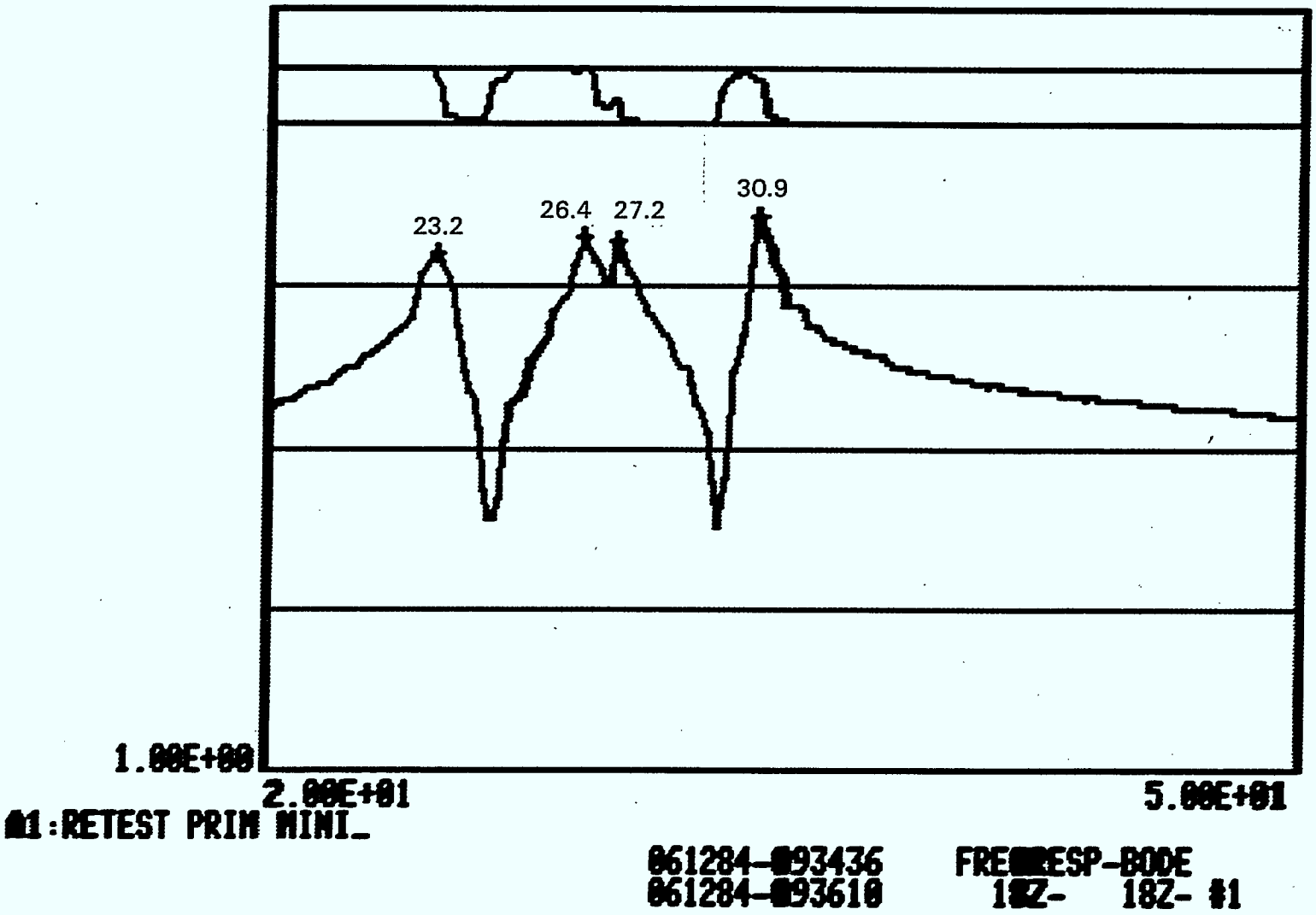

FIGURE 5-16 PRIMARY STRUCTURE EXPERIMENTAL FRF (MINI SHAKER, RETEST)

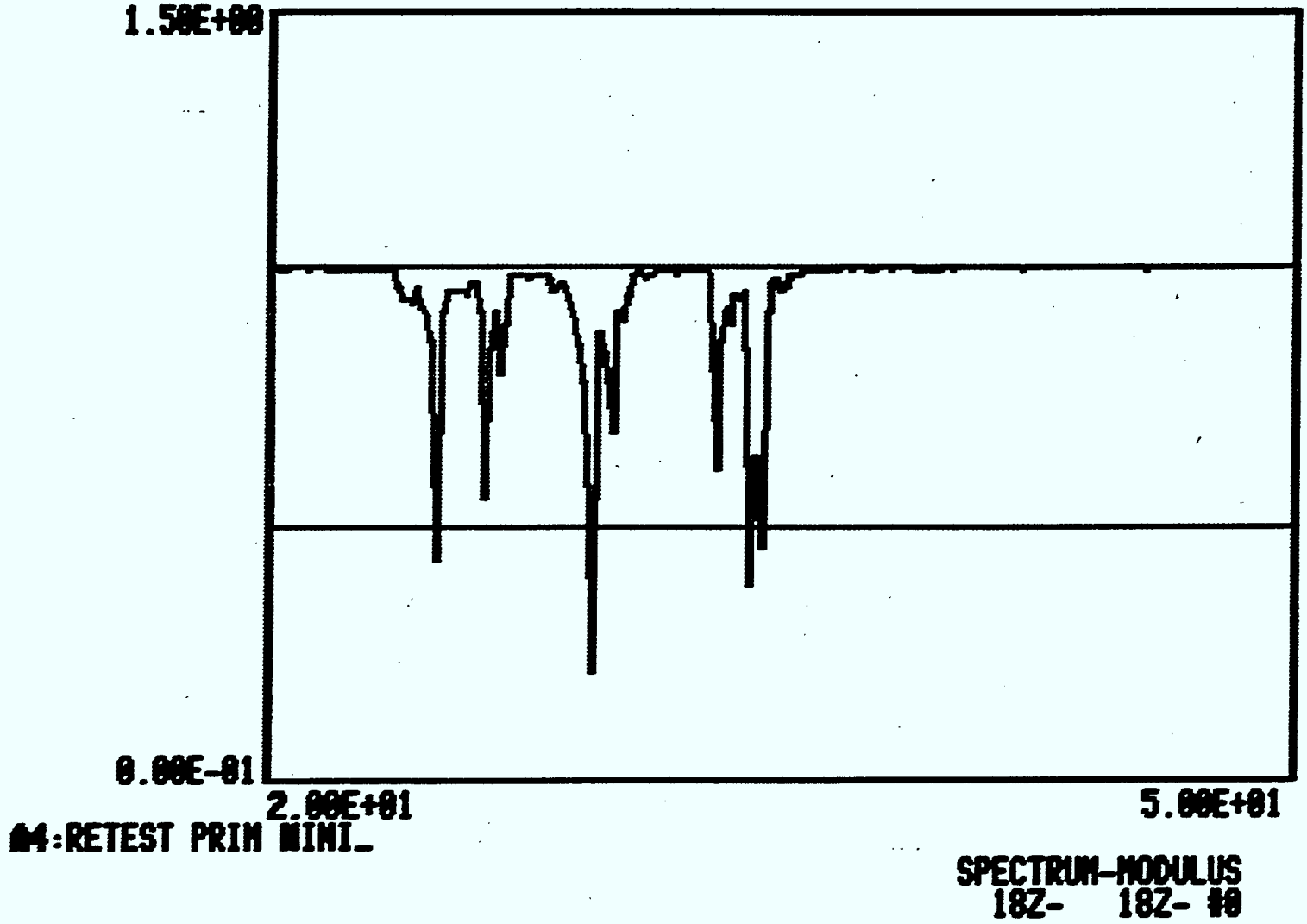

FIGURE 5-17 PRIMARY STRUCTURE COHERENCE FUNCTION (MINI SHAKER, RETEST)

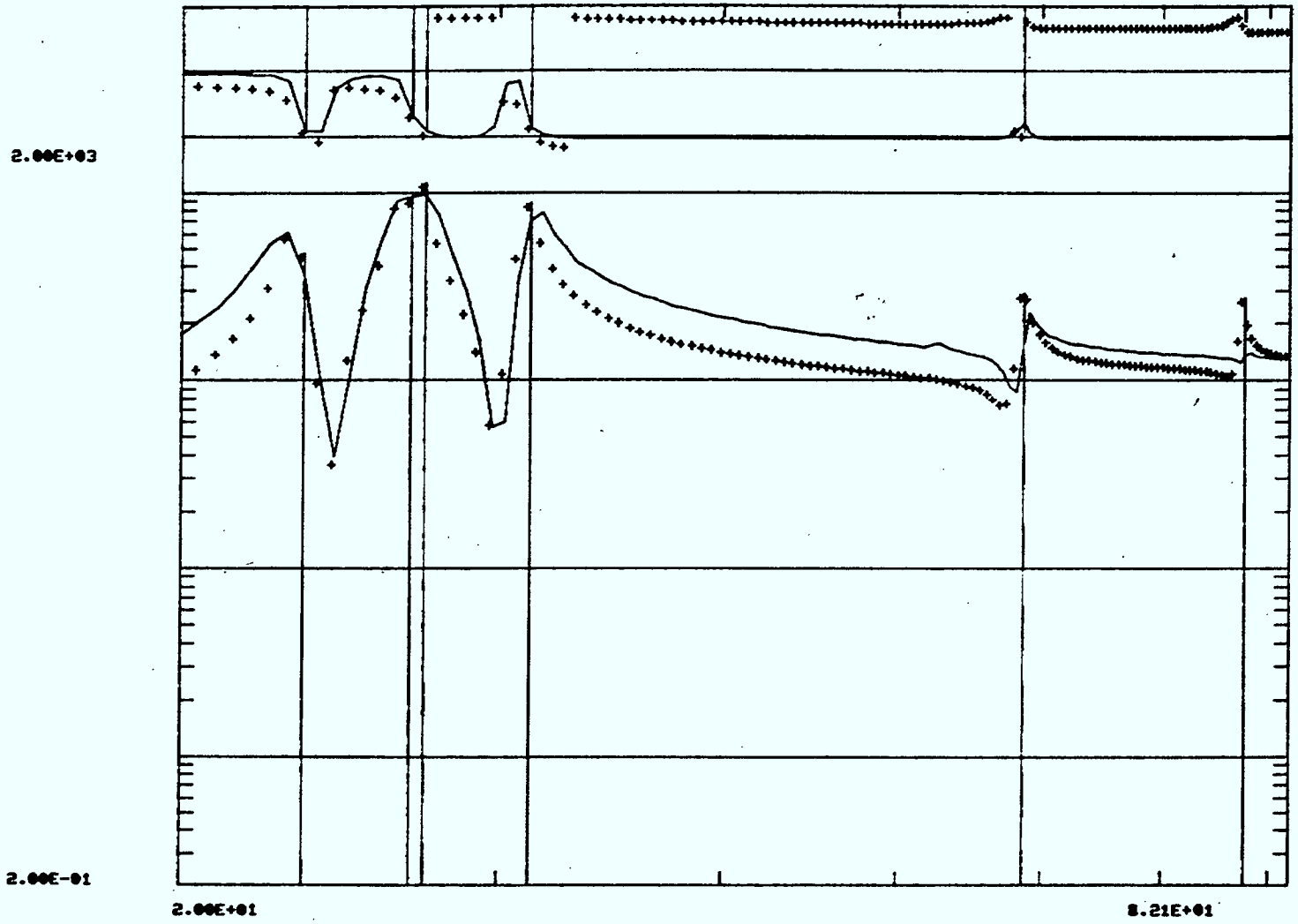

FIGURE 5-18 POLYREFERENCE CURVE FIT - MINI SHAKER EXCITATION

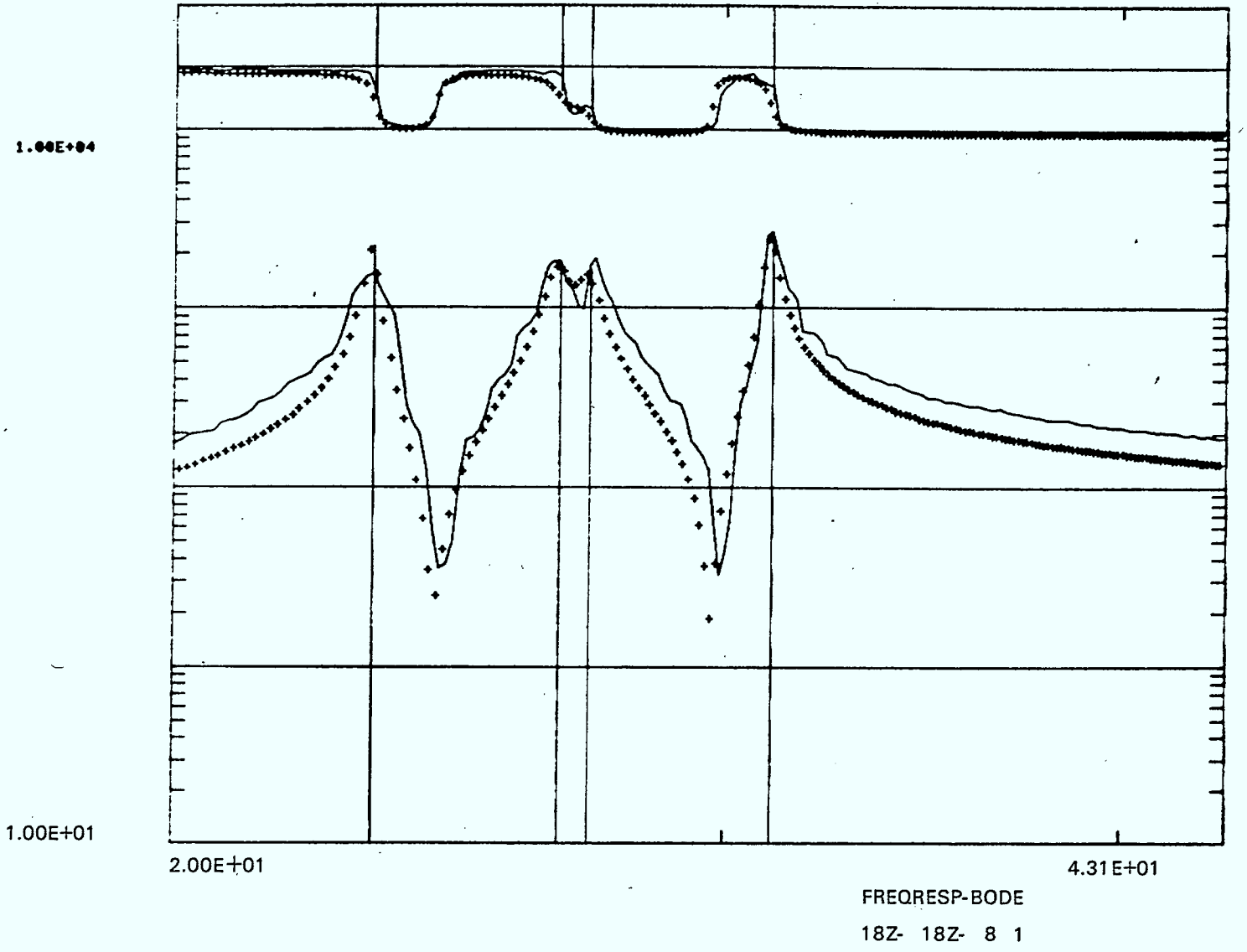

FIGURE 5-19 CURVE FIT ZOOMED

TABLE 5-1

BASE EXCITATION TEST PARAMETERS

(PRIMARY STRUCTURE)

EXCITATION	TEST AXIS	FREQUENCY RANGE	SWEEP RATE	NO. OF AVERAGES
Sine	Z	20-160 Hz	.5 Oct/min.	113
Random (pseudo)	X	10-400 Hz	na	40
Random (pseudo)	Z	10-400 Hz	na	40

TABLE 5-2(a)

TEST CONFIGURATION: SINE SWEEP, UNCORRECTED FRF, Z-AXIS

FREQUENCY (HZ)	DAMPING (Z)	DESCRIPTION OF MODE
23.127	0.9	Semi symmetric plate mode.
25.085	0.7	Shelf rotates about Y axis and bends thrust cone.
26.227	4.0	Not calculated.
26.903	0.6	Anti symmetric plate mode.
27.627	6.0	Anti symmetric plate mode.
30.869	0.7	Symmetric plate mode.
75.555	0.8	Drum mode.
98.184	0.7	Shelf moves in plane in Y direction.
133.888	0.5	Out of plane shelf mode.
145.95	0.5	Out of plane shelf mode.

TABLE 5-2(b)

TEST CONFIGURATION: SINE SWEEP; CORRECTED FRF'S; Z-AXIS

FREQUENCY (HZ)	DAMPING (%)	DESCRIPTION OF MODE
23.291	1.0	Not calculated
25.199	1.6	Not calculated
26.783	1.9	Not calculated
27.047	2.2	Not calculated
30.781	1.8	Symmetric shelf mode
75.764	1.2	Drum mode

TABLE 5-3(a)

TEST CONFIGURATION: RANDOM; UNCORRECTED FRF'S; X-AXIS

FREQUENCY Hz	DAMPING (%)	DESCRIPTION OF MODE
85.499	4.6	Thrust tube torsion inducing buckling type deflection in shelf.
104.492	1.8	Thrust tube torsion inducing buckling type deflection in shelf (same as above mode but in perpendicular direction).
178.873	1.1	Large out of plane deflection at point 42.
204.111	2.1	Large in plane deflection at point 21.

TABLE 5-3(b)

TEST CONFIGURATION: RANDOM; UNCORRECTED FRF'S; Z-AXIS

FREQUENCY	DAMPING	DESCRIPTION OF MODE
30.51	1.2	N/C
75.88	0.5	N/C
85.56	4.6	N/C
104.5	1.9	N/C
139.2	2.4	N/C
162.3	1.3	N/C
177.2	6.6	N/C
179.6	1.2	N/C
198.2	3.3	N/C
203.7	1.1	N/C
246.3	2.6	N/C

TABLE 5-4

COMPARISON OF RANDOM AND SINE SWEEP RESULTS FOR BASE EXCITATION CONFIGURATION

SINE SWEEP Z-AXIS UNCORRECTED FRF'S		SINE SWEEP Z-AXIS CORRECTED FRF'S		RANDOM Z-AXIS UNCORRECTED FRF'S		RANDOM X-AXIS UNCORRECTED FRF'S	
FREQUENCY	DAMPING	FREQUENCY	DAMPING	FREQUENCY	DAMPING	FREQUENCY	DAMPING
23.127	0.9	23.291	1.0	N/C	N/C		
25.085	0.7	25.199	1.6	N/C	N/C		
26.227	4.0			N/C	N/C		
26.903	0.6	26.783	1.9	N/C	N/C		
27.627	6.0	27.047	2.2	N/C	N/C		
30.869	0.7	30.781	1.8	30.51	1.2		
75.555	0.8	75.764	1.2	75.88	0.5		
				85.56	4.6	85.499	4.6

TABLE 5-4 - Continued

COMPARISON OF RANDOM AND SINE SWEEP RESULTS FOR BASE EXCITATION CONFIGURATION

SINE SWEEP Z-AXIS UNCORRECTED FRF'S		SINE SWEEP Z-AXIS CORRECTED FRF'S		RANDOM Z-AXIS UNCORRECTED FRF'S		RANDOM X-AXIS UNCORRECTED FRF'S	
FREQUENCY	DAMPING	FREQUENCY	DAMPING	FREQUENCY	DAMPING	FREQUENCY	DAMPING
98.184	0.7	N/C	N/C				
				104.5	1.9	104.492	1.8
133.888	0.5	N/C	N/C				
				139.2	2.4		
145.95	0.5	N/C	N/C				
				162.3	1.3		
				177.2	6.6	178.873	1.1
				179.6	1.2		
				198.2	3.3		
				203.7	1.1	204.111	2.1
				246.3	2.6		

TABLE 5-5

MINI SHAKER TEST CONDITIONS - PRIMARY STRUCTURE

EXCITATION POINT	FREQUENCY RANGE	NO. OF AVERAGES	TEST SERIES
15 Tangential -	10-250 Hz.	40	First
15 Z -	10-250 Hz.	40	First
19 Radial	10-250 Hz.	40	First
19 *	10-250 Hz.	40	First
18 Z-	10-250 Hz.	25	Retest
19 Tangential	10-250 Hz.	25	Retest
19 *	10-250 Hz.	25	Retest

* skewed input; angle to X, Y axis = 45°
angle to Z axis = 32°

TABLE 5-6

MINI-SHAKER PARAMETERS

FREQUENCY	DAMPING	PHASE	AMPLITUDE
23.222	1.1 %	1.015	1205
26.709	0.9	0.940	1772
27.109	0.8	1.528	1642
31.101	1.1	1.314	1840
58.692	0.7	0.462	602
77.501	0.4	-0.005	363

TABLE 5-7(a)

TEST SERIES: 1ST MINI-SHAKER; REFERENCE COORDINATES 150 19R

FREQUENCY	DAMPING	MODAL MASS	DESCRIPTION OF MODE
23.138	1.3	2.4×10^4	Semi symmetric shelf mode
26.862	0.9	1.2×10^5	Anti symmetric shelf mode
30.984	0.9	5.2×10^4	Symmetric shelf mode
77.020	0.5	N/C	Drum mode
86.103	3.3	58	In plane shelf mode
87.183	1.1	2.0×10^4	Thrust cone bending in Y direction (about X-axis)
87.518	0.8	9.3	Shelf deforming in plane.
87.574	4.8	.721	Not calculated.
104.506	1.2	N/C	Not calculated
105.424	0.8	N/C	Not calculated
105.680	0.5	N/C	Not calculated
107.757	3.7	N/C	Not calculated

TABLE 5-7(b)

TEST SERIES: RETEST MINI-SHAKER; REFERENCE COORDINATES 18Z 190

FREQUENCY	DAMPING	MODAL MASS	DESCRIPTION OF MODE
23.183	1.8	3.5×10^2	Semi-symmetric shelf mode
26.697	0.8	1.5×10^4	Anti-symmetric shelf mode
27.447	1.3	2.5×10^1	Anti-symmetric shelf mode
31.388	2.7	4.3×10^1	Symmetric shelf mode
57.643	1.1	4.4×10^2	Half of shelf moves out of plane
77.515	0.4	9.3×10^2	Drum mode
86.385	0.9	2.7×10^4	Thrust cone bending (X & Y direction)
105.969	0.4	1.4×10^5	Shelf shearing about Z-axis (twist)
106.508	1.0	2.4×10^3	Shelf shearing in opposite direction to mode at 105.969 Hz.
111.291	0.8	2.1×10^4	Thrust cone twisting
134.626	0.5	1.4×10^4	Not calculated
138.504	0.6	2.6×10^3	Not calculated
149.311	1.2	1.0×10^5	Not calculated
166.752	1.0	3.1×10^4	Not calculated
169.300	1.6	9.2×10^3	Not calculated
172.384	0.3	2.6×10^6	Not calculated

TABLE 5-8

COMPARISON OF MINI-SHAKER TEST RESULTS

1ST MINI-SHAKER TEST		MINI-SHAKER RETEST		ZOOMED FUNCTIONS FROM RETEST	
FREQUENCY	DAMPING	FREQUENCY	DAMPING	FREQUENCY	DAMPING
23.138	1.3	23.183	1.8	23.248	0.5
26.862	0.9	26.697	0.8	26.618	0.9
		27.447	1.3	27.194	0.8
30.984	0.9	31.388	2.7	31.047	0.5
		57.643	1.1	N/C	N/C
77.020	0.5	77.515	0.4	N/C	N/C
86.103	3.3	86.385	0.9	N/C	N/C
87.183	1.1	N/C	N/C	N/C	N/C
87.518	0.8	N/C	N/C	N/C	N/C
87.574	4.8	N/C	N/C	N/C	N/C

TABLE 5-9

PRIMARY STRUCTURE COMPARISON OF FREQUENCY AND DAMPING RESULTS FOR VARIOUS TEST CONFIGURATIONS

BASE EXCITATION						MINI-SHAKER EXCITATION TO SHELF			
SWEEP (Z-AXIS) 20-160 HZ		RANDOM (X-AXIS) 10-400 HZ		RANDOM (Z-AXIS) (10-400 HZ)		1ST TEST 4 POINTS OF EXCITATION (10-200 HZ)		RETEST 2 POINTS OF EXCITATION (10-200 HZ)	
FREQUENCY (HZ)	DAMPING (%)	FREQUENCY (HZ)	DAMPING (%)	FREQUENCY (HZ)	DAMPING (%)	FREQUENCY (HZ)	DAMPING (%)	FREQUENCY (HZ)	DAMPING (%)
23.291	1.0					23.138		23.248	0.5
25.085	0.7								
26.903	0.6					26.862	0.9	26.618	0.9
27.047	2.2							27.194	0.8
30.869	0.7			30.51	1.1	30.984	0.9	31.047	0.5
								57.643	1.1
75.555	0.8			75.88	0.5	77.020	0.5	77.515	0.4
		85.499	4.6	85.56	4.6	87.183	1.1	86.385	0.9
						87.518	0.8		
						87.574	4.8		
		104.492	1.8	104.5	1.9			105.969	0.4
								106.508	1.0
								111.771	0.4
133.888	0.5							134.130	0.8
								134.626	0.5

6.0 COUPLED STRUCTURE TESTS

The coupled structure was comprised of the primary and secondary structures, joined together. The justification for the coupled structure test was the verification of the analytical coupling procedures. The number of degrees of freedom (number of accelerometers) needed was not as great as that of the primary structure, though there were many more modes present over the same frequency range.

6.1 TEST CONFIGURATION

The coupled structure was tested in a fixed-free configuration using mini-shaker input. Four different excitation points were used, two of them were chosen for parameter estimation.

The structure was instrumented with 55 accelerometers. Less accelerometers were used for this test than the primary because the results were not necessary for the substructure coupling analysis - they were only to be used to verify the substructure coupling analysis.

Figures 6-1 and 6-2 show the accelerometer degrees of freedom and locations. The coordinate of the points are the same as those used in the primary and secondary structures. Table 6-1 lists the test conditions.

6.2 TEST RESULTS

Figure 6-3 is a frequency response function taken from point 23Z, located at the tip of the secondary structure. It appears much busier than those for the primary or secondary structure, because it combines the modes of both structures. The first mode is a secondary structure bending mode. The frequency was 14.8 Hz, compared to the free-free frequency of 30 Hz.

The coherence function, Figure 6-4 shows many sharp dips below 1. In the low frequency regime some of the dips are due to insufficient frequency resolution. Many of the other dips are associated with anti-resonances.

Table 6-2 list the modal parameters predicted by POLYREFERENCE processing. The shelf modes show very similar values to those of the primary structure alone (frequency and damping). The secondary structure frequency values are much lower due to the test configuration, but the damping values are very similar.

The values listed in Table 6-2 were chosen from the predicted parameters based on modal assurance criteria. Tables 6-3(a) and b list the modal assurance criteria.

Figure 6-5 shows the first bending mode of the secondary structure. It is not the same shape as that of the free-free mode, and it has caused some deflection of the primary structure shelf.

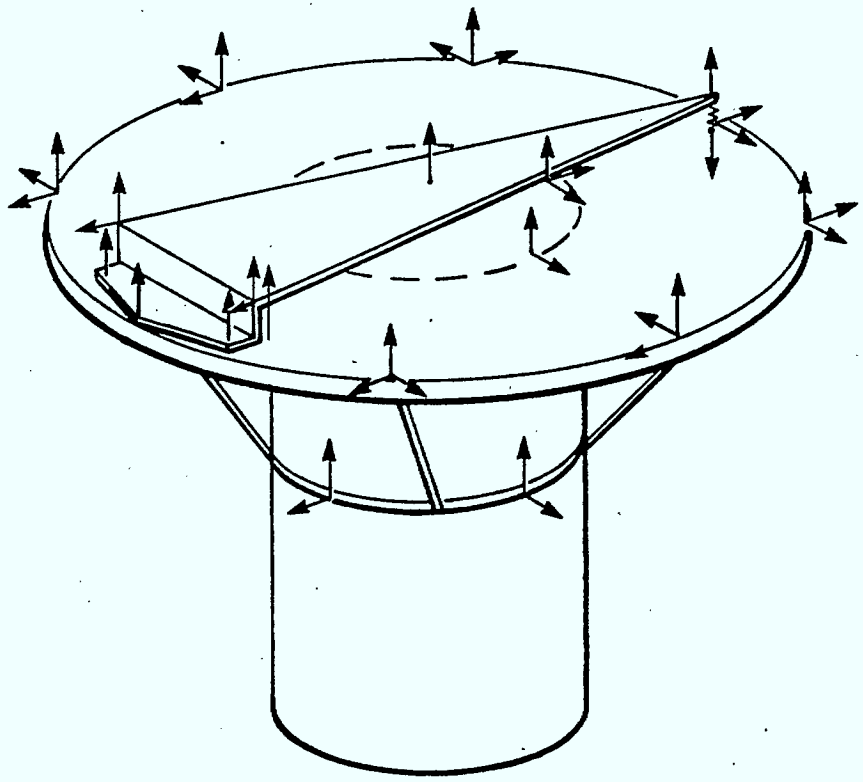

FIGURE 6-1 T-SAT COUPLED STRUCTURE GEOMETRY COORDINATES

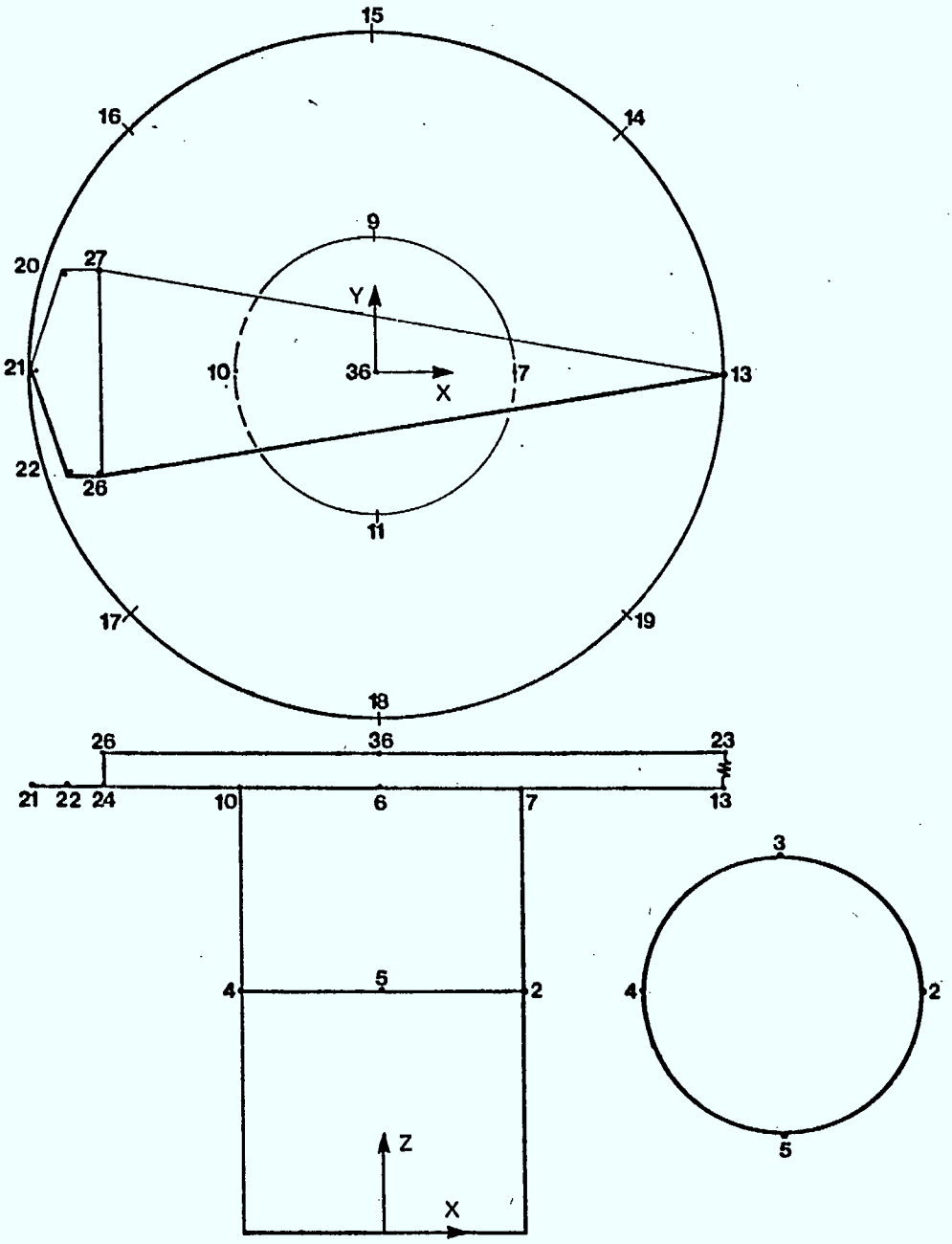

FIGURE 6-2 T-SAT COUPLED STRUCTURE GEOMETRY COORDINATES

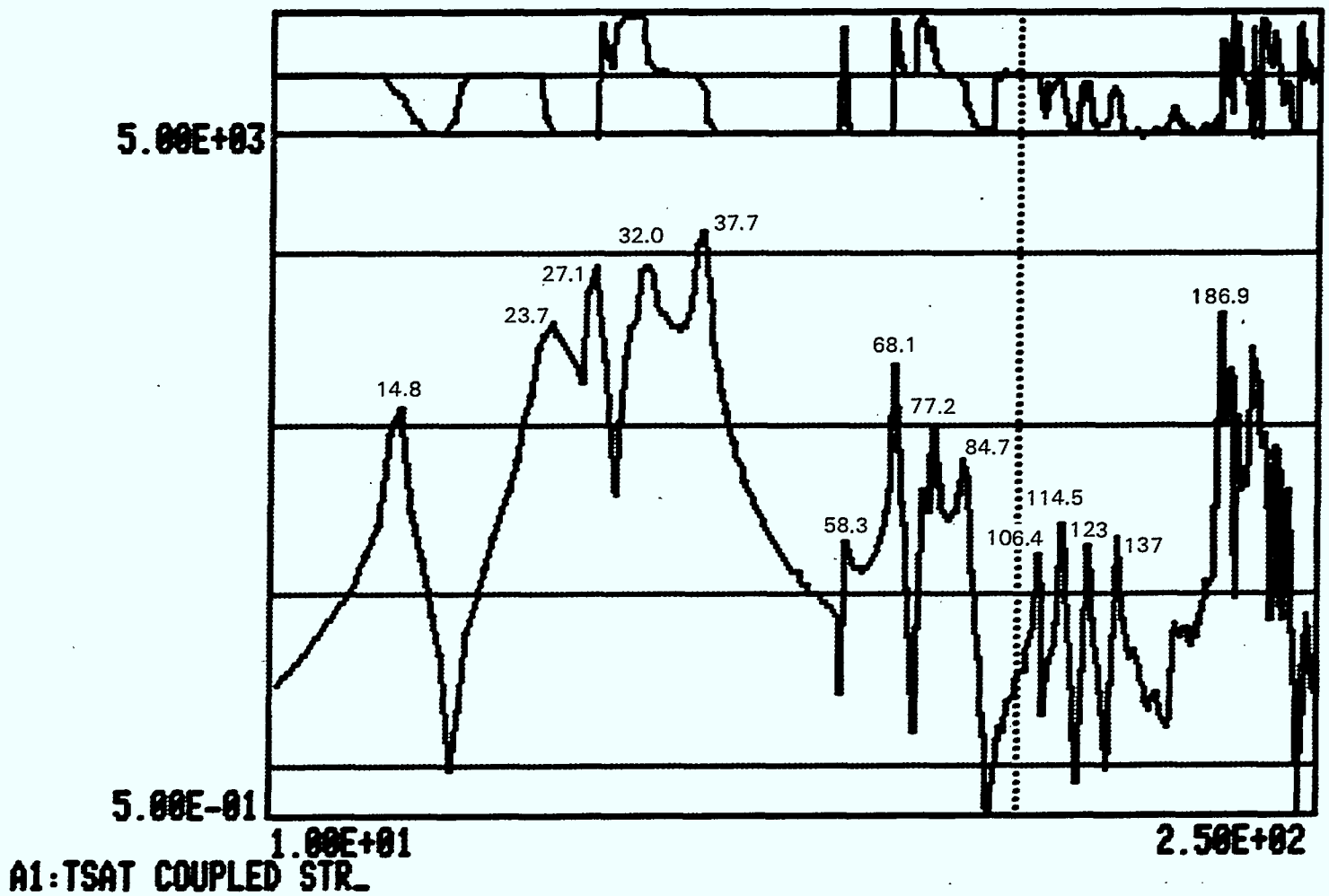

FIGURE 6-3 COUPLED STRUCTURE EXPERIMENTAL FRF (MINI SHAKER)

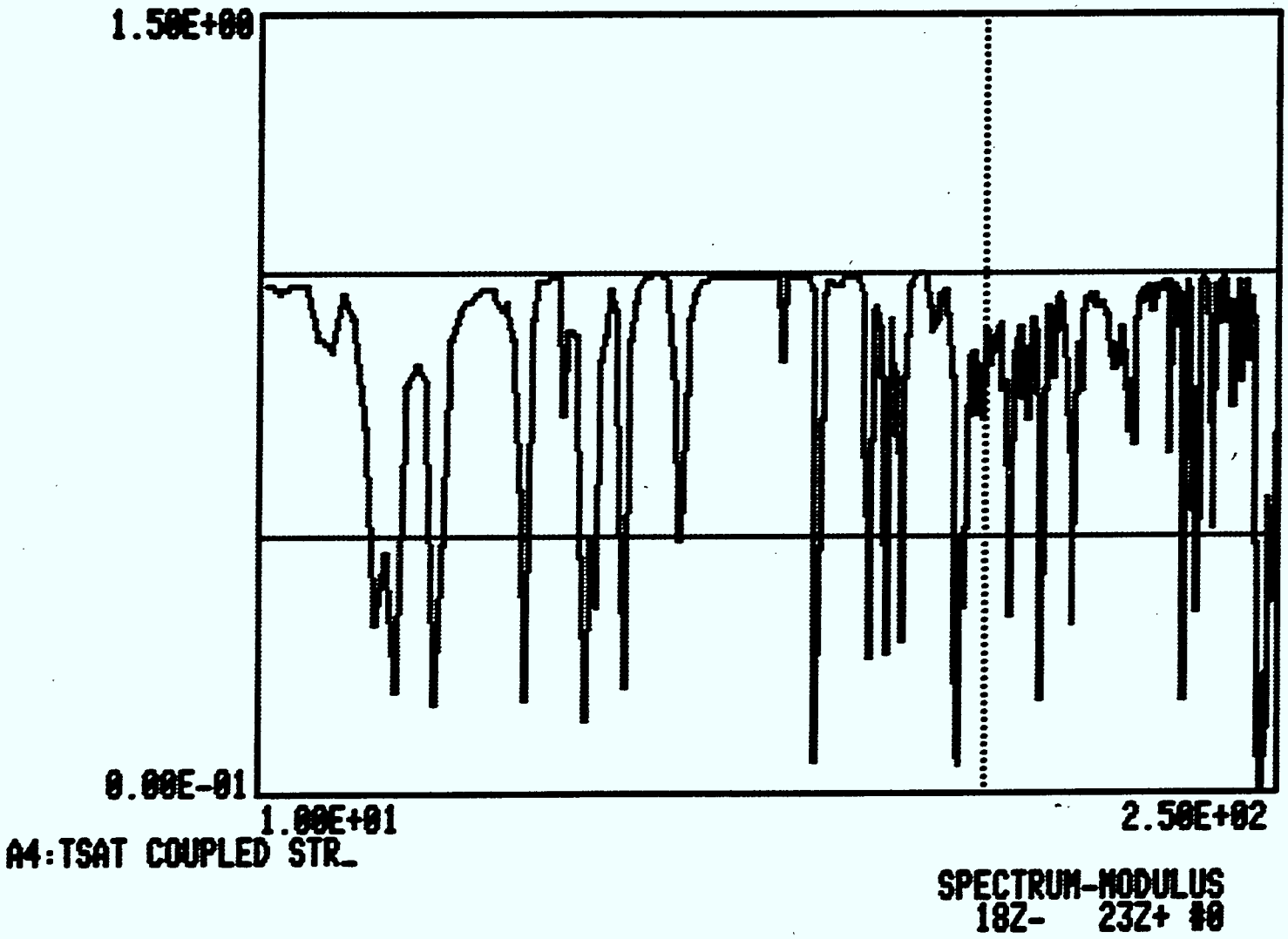

FIGURE 6-4 COUPLED STRUCTURE COHERENCE FUNCTION (MINI SHAKER)

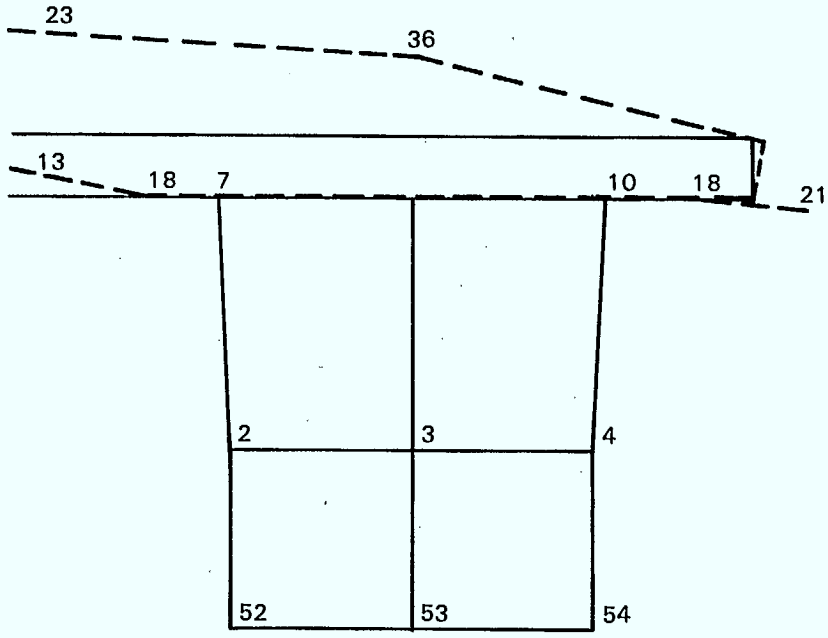

FIGURE 6-5 COUPLED STRUCTURE - 1ST MODE 15.1 Hz

TABLE 6-1

MINI-SHAKER TEST CONDITIONS - COUPLED STRUCTURE

EXCITATION POINT	FREQUENCY RANGE	NO. OF AVERAGES
18 Z-	10-250 Hz.	25
19 Radial	10-250 Hz.	25
19 Tangential	10-250 Hz.	25
19 *	10-250 Hz.	25

* skewed input; angle to X, Y axis = 45°
angle to Z axis = 32°

TABLE 6-2

COUPLED STRUCTURE RESULTS

FREQUENCY (HZ)	DAMPING (%)	MODE	DESCRIPTION OF MODE
15.1	2.2	1	1ST BENDING OF SECONDARY STRUCTURE
23.5	1.0	2	SEMI-SYMMETRIC PLATE MODE; SECONDARY STRUCTURE BENDING
26.6	0.6	3	ANTI-SYMMETRIC PLATE MODE
28.0	1.2	4	ANTI-SYMMETRIC PLATE MODE
32.0	1	5	SYMMETRIC PLATE MODE; SECONDARY STRUCTURE BENDING
33.6	1.3	6	SYMMETRIC PLATE MODE; SECONDARY STRUCTURE TWISTING
37.6	2.6	7	SECONDARY STRUCTURE BENDING
69.5	0.4	8	SECONDARY STRUCTURE BENDING
71.9	3.2	9	SECONDARY STRUCTURE FLANGE BENDING

TABLE 6-2 - Continued

FREQUENCY (HZ)	DAMPING (%)	MODE	DESCRIPTION OF MODE
76.2	0.5	10	SECONDARY STRUCTURE TWISTING
77.7	0.4	11	PLATE DRUM MODE
79.9	5.4	12	THRUST TUBE BENDING; SECONDARY STRUCTURE TWISTING
85.1	1	13	THRUST TUBE BENDING; SECONDARY STRUCTURE FLANGE BENDING
95.4	4.8	14	ONE QUADRANT OF PLATE BUCKLING
105.3	3	15	TWIST IN PLANE OF PLATE
106.8	0.7	16	SECONDARY STRUCTURE FLANGE BENDING
107.	1.7	17	THRUST CONE TWISTING

TABLE 6-2 - Continued

FREQUENCY (HZ)	DAMPING (%)	MODE	DESCRIPTION OF MODE
114.8	0.6	18	SECONDARY STRUCTURE BENDING; THRUST CONE BENDING
123	0.9	19	SECONDARY STRUCTURE TWISTING ABOUT X-AXIS
126.	9.0	20	SHELF MODE
130.	3.4	21	SHELF MODE
137.	0.8	22	THRUST CONE BENDING; SHELF DEFLECTING OUT OF PLANE
143.	1.1	23	SHELF MODE
150.	1.8	24	THRUST CONE BENDING; SHELF DEFLECTING OUT OF PLANE
162	1.3	25	THRUST CONE TWISTING
168	1.3	26	SYMMETRIC SHELF MODE
170	0.3	27	SECONDARY STRUCTURE BENDING

	1	2	3	4	5	6	7	8	9	10	11	12	FREQ.	ζ
1	1	.09	.03	.03	0	0							15.12	.022
2		1	.06	.27	0	.18							18.43	.103
3			1	.56	.49	.14							21.56	.152
4				1	.64	.04	.18	0	.18				23.34	.005
5					1	0	.09	.02	.08				23.54	.010
6						1	.76	.13	0				26.65	.006
7							1	.25	0	0	.02	.04	27.51	.024
8								1	.06	.03	.09	.07	27.97	.012
9									1	.90	.02	.15	31.71	.003
10										1	.01	22	31.99	.010
11											1	.24	33.57	.013
12												1	37.61	.026

TABLE 6-3(a) COUPLED STRUCTURE MODAL ASSURANCE CRITERIA (PART 1)

	1	2	3	4	5	6	7	8	9	10	11	12	FREQ.	ζ
1	1	.09	0	.02	.04	.03							69.54	.005
2		1	.17	.12	.04	.01							71.16	.032
3			1	.06	.15	.59							76.16	.005
4				1	.01	0	.04	.08	.38				76.18	.088
5					1	.03	.01	.01	0				77.73	.004
6						1	.15	.08	.41				79.88	.054
7							1	.96	.02	.13	0	.02	85.10	.009
8								1	0	.17	0	.02	85.62	.010
9									1	.51	.34	.02	94.09	.039
10										1	.15	0	95.40	.049
11											1	.01	105.25	.029
12												1	106.83	.007

TABLE 6-3(b) COUPLED STRUCTURE MODAL ASSURANCE CRITERIA (PART II)

7.0 CONCLUSIONS

The testing exercise within this contract has increased the modal test capability at DFL and Spar to include all aspects of the phase separation techniques, with the exception of those involving multiple inputs.

The requirement to provide the data for substructure coupling work uncovered many factors which might otherwise have been overlooked. In previous test exercises the importance of modal mass and residual corrections were not considered. The mounting requirements for a free-free test configuration were not understood until the results were compared with a FEM. In turn, the FEM modelling requirements were not adequate until test results were examined.

The development of a capability for mini-shaker testing is not yet complete. The processing and testing time required to achieve results comparable to the base excitation is still excessive. Advancement to multi-shaker input testing should solve time problems.

The testing and processing of the results described in this report took about 5 months. There were several reasons for such a long duration. Two key factors included the data acquisition system and the lack of test priority at DFL. The data acquisition system is slated to be upgraded. The test priority was frustrating, but is not something that would be a problem for tests on flight hardware. The requirement for two groups to provide results for one another accounted for almost a month of the five month period. Though this interface was time-consuming for both sides, it did generate additional understanding of the methods.

At the completion of the exercise, there were still areas of uncertainty in both test results and FEM results. The FEM was unable to predict one major mode. The test results included modes that could have been numerical in nature only, but the software could not verify this.

Had more time been available, a retest of the structure, concentrating on the questionable modes could have eliminated the uncertainty.

The secondary structure was tested in a free-free configuration, to accommodate the limitations of the substructure program to be used in the subsequent coupling exercise. Some of the coupling results could probably have been improved with a constrained mode test (to more accurately simulate the load path).

The coupling work that followed this experimental work showed promise for establishing a modal data base, to replace the tradition FEM modal data base.

The use of experimental data in the substructure analysis provides more representative data. By virtue of the fact that it is based on the actual structure, many assumptions made by the structural analyst can be eliminated. In comparing the first NASTRAN model made of the primary structure to the experimental modal results, significant modelling errors were detected. These included the method of connection of a large mass to the structure (which induced an error in frequency of approximately 20 Hz) as well as smaller errors concerning actual dimensions vs reported dimensions.

In the secondary structure tests, the FEM mass distribution introduced an error of about 30% of the torsion frequencies. Conversely, the modal test boundary conditions initially introduced an error of about 10 Hz in the first bending mode, which the FEM was able to detect. The problem of appropriate boundary conditions is a serious one, both for free-free or fixed-free tests.

All modes from the test of the primary structure, which was tested using both base excitation and single input force input, were determined using either method. The portable shaker (single input force) did a better job of exciting the first three modes of the structure, but a poor job of exciting one of the more dominant modes (the drum mode). The base excitation sine test seemed slightly superior to the random test, with respect to exciting the more subtle modes.

In an investigation of base excitation testing, (done by CRC and University of Sherbrooke personnel, as well as SPAR RMSD), several important facts about the processing software were discovered. Processing of computer generated information (i.e. known modal parameters) provided an insight into the POLYREFERENCE algorithm.

The base excitation results themselves were very promising and certainly it is worth developing a method to extract modal mass information so that the results can be used for substructure coupling. The conclusion of this contract will involve developing such a technique, though its experimental verification remains as a future task.

There are a number of areas of modal testing and analysis that need further investigation. These include:

(a) Multiple input mini shaker testing.

(b) Residual flexibility effects.

(c) Boundary condition effects.

(d) Improvement of modal mass estimation.

(e) Statically indeterminant interface conditions.

(f) Development of a base excitation software package.

BIBLIOGRAPHY

(1) "Modelling and Identification of the Structural Properties of an Astromast", Y. Soucy and F. Vigneron, CRC Report, November 1983.

(2) "Modal Survey Test on the Seismic Block", T. Steele and F. Vigneron, CRC-DSM File 5440-4, April 1984.

(3) MODAL PLUS Users Manual, Structural Dynamics Research Corporation, Version 8, 1983.

(4) "Modal Parameter Estimation from Base Excitation Data", J.G. Beliveau, F.R. Vigneron, Y. Soucy and S. Draisey, to be submitted to ASME.

(5) Course Notes from University of Cincinnati, Modal Analysis Lectures, 1983.

(6) "Validation of Substructure Coupling Technique for Structure Verification Using SPRC Software", SPAR-RML-009-84-172, 1984.

APPENDIX A

MODAL MASS

From finite element models, modal mass is calculated as $M = \phi^T [m] \phi$ where $[m]$ represents the physical mass matrix.

ϕ represents the matrix of eigenvectors.

Thus for each eigenvalue (or for each mode) there is a single number which represents the modal mass.

For any mode, the eigenvector represents a ratio of the displacements of the points, thus the eigenvector can be multiplied by any scaling constant. The same scaling constant is present for the calculation of modal mass.

For example, consider the system in Figure A-1.

If the eigenvector were to be rescaled such that the modal mass was equal to 1, the mode 1 result would be $\phi / \sqrt{1.801} =$

$$\begin{matrix} .745 \\ .480 \\ .223 \end{matrix}$$

The modal mass and the eigenvectors can be scaled by any number, but the relationship between them must remain unchanged.

In the case where the eigenvector has been scaled such that the maximum displacement is 1, the modal mass cannot exceed the mass of the structure.

For rigid body motion, the mass and the modal mass are equal.

In experimental modal analysis, all of the above rules apply - only the method of determining the value of the modal mass is different.

Consider the equation of motion, for resonance r, decoupled by transformation to modal coordinates (proportional damping assumed)

$$M_r \ddot{q}_r + C_r \dot{q}_r + K_r q_r = f_r(t) \quad \text{where } f_r'(t) = [\phi_r]^T [f(t)]$$

taking the Laplace, it becomes

$$(s^2 M_r + s C_r + K_r) Q_r(s) = F'(s)$$

$$Q_r(s)/F'(s) = (1/M_r)/(s^2 + s(C_r/M_r) + (K_r/M_r))$$

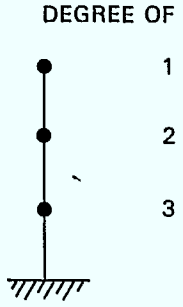

$$[m] = \begin{bmatrix} 1 & 0 & 0 \\ 0 & 1.5 & 0 \\ 0 & 0 & 2 \end{bmatrix}$$

THE EIGENVALUES

$$\begin{bmatrix} W_1{}^2 \\ W_2{}^2 \\ W_3{}^2 \end{bmatrix} = \begin{bmatrix} 210 \\ 966 \\ 2124 \end{bmatrix}$$

THE EIGENVECTORS

$$\phi = \begin{bmatrix} 1.0 & 1.0 & 1.0 \\ 0.644 & -0.601 & -2.57 \\ 0.300 & -.676 & 2.47 \end{bmatrix}$$

THE MODAL MASS FOR MODE 1

$$[1. \quad .644 \quad 0.300] \begin{bmatrix} 1 & 0 & 0 \\ 0 & 1.5 & 0 \\ 0 & 0 & 2 \end{bmatrix} \begin{bmatrix} 1 \\ .644 \\ .300 \end{bmatrix} = 1.802$$

FIGURE A-1 MODAL DEGREES OF FREEDOM

Which can also be written:

$$H(s) = Q_r(s)/F'(s) = (1/M_r)/((s-P_r)(s-P_r^*))$$
$$= (A_{1r}/(s-P_r) + A_{2r}/(s-P_r^*)$$

Where: $P_r = \sigma_r + i\, w_{rd}$
$= \sigma_r W_r + w_{rd}$
$= (C_r/C_{cr})w_r + i\, w_{rd}$

$$H(s)\,(s-P_r) = A_{1r} + ((s-P_r)/(s-P_r^*))A_{2r}$$

And evaluate at $s = p_r$

$$A_{1r} = (1/M_r)/(P_r-P_r^*)$$

$P_r = \sigma + iw_d$
$P_r^* = \sigma - iw_d$

$$A_{1r} = (1/M_r)/(2iw_d)$$

$$M_r = (1/(A_{1r}\ 2iw_d))$$

However, this solution is in terms of modal degrees of freedom [$Q_r(s)$ and $F'(s)$] while the frequency response information is available in terms of physical degrees of freedom [$X_r(s)$ and $F_r(s)$].

The relationship for displacement at point i is:

$$X_{ir} = \phi_{ir} Q_r$$

For a single forcing point j:

$$F_r' = \phi_r^T \begin{Bmatrix} \phi \\ \vdots \\ F_j \\ 0 \\ \vdots \\ 0 \end{Bmatrix}$$

$$= \phi_j F_j$$

the frequency response function $H_{ij} = \frac{X_i}{F_j}$
(at resonance r)

$$= \phi_i^r \, Q_r/(F_r'/\phi_j)$$

$$= \phi_{ir}\phi_{jr}(Q_r/F_r')$$

Thus: $Q_r F_r' = H_{ij}/(\phi_i\phi_j)$

and therefore the residue A_r, measured in physical coordinates must be divided by $\phi_i\phi_j$ to calculate the modal mass.

$$\frac{A_{lr}}{\phi_i\phi_j} = \frac{1/M_r}{2iw_d}$$

$$M_r = \frac{\phi_i\phi_j}{A_{ir} \, 2 \, iw_d}$$

If the FRF is measured in terms of acceleration rather than displacement, the result must be multiplied by w_r^2

APPENDIX B

Appendix B - Modal Assurance Criterion (MAC) Ref. 5

Modal Assurance Criterion is used to determine if multiple eigenvalues, predicted at the same or very close frequencies, have two independent sets of eigenvectors. it is essentially the square of the correlation coefficient between the two (or multiple) shapes.

Figure B-1 shows the residue matrix for a particular mode r, which has been established from three reference (excitation) points. Examination of the three columns indicates that they are just linear combinations of one another. For example the second column equals the first column times $\frac{U(2,r)}{U(1,r)}$.

If the parameter estimation software has predicted more than one eigenvalue equal to that of mode r, the MAC can be used to determine if there are several eigenvalues at the same frequency or if they are in fact the same mode, with eigenvectors which are not independent.

Figure B-2 lists the equations which are used to determine the modal assurance criterion. MAC is the modal assurance criterion, which represents a number for each of the modes compared.

Figure B-3 is an example of a modal assurance criteria matrix comparing six modes of the secondary structure. A value of zero indicates that there is no linear dependence between the two modes. A value of 1 indicates a linear relationship between the two.

The modal assurance criterion should not be confused with an orthogonality check. In the case of an orthogonality check, the eigenvectors are <u>weighted</u> by the <u>mass matrix</u> to determine if the two eigenvectors are orthogonal to one another. An orthogonality check applies to any of the eigenvectors, while MAC should only be used to compare eigenvectors which potentially represent the same mode.

MAC is not a conclusive criteria, it can appear artificially low if the system tested is non-stationary or non-linear, there is noise present in the input or the parameter estimation is invalid.

MAC can also appear artificially high (indicating a linear relationship where none exists), if there is a coherent noise source present during test there were insufficient degrees of freedom to define the mode, there are more inputs to the system than those considered.

Modal Assurance Criterion cannot be used to eliminate all of the spurious modes predicted by phase separation types of software, but it does help to eliminate some.

RESIDUE MATRIX, A(r) FOR MODE r

$$[A(r)] = k(r) \begin{bmatrix} U(1,r)\,U(1,r) & U(1,r)\,U(2,r) & U(1,r)\,U(3,r) \\ U(2,r)\,U(1,r) & U(2,r)\,U(2,r) & U(2,r)\,U(3,r) \\ U(3,r)\,U(1,r) & U(3,r)\,U(2,r) & U(3,r)\,U(3,r) \\ U(4,r)\,U(1,r) & U(4,r)\,U(2,r) & U(4,r)\,U(3,r) \\ U(5,r)\,U(1,r) & U(5,r)\,U(2,r) & U(5,r)\,U(3,r) \\ U(6,r)\,U(1,r) & U(6,r)\,U(2,r) & U(6,r)\,U(3,r) \\ U(7,r)\,U(1,r) & U(7,r)\,U(2,r) & U(7,r)\,U(3,r) \end{bmatrix}$$

WHERE: k(r) IS A SCALING CONSTANT FOR MODE r

u(i, r) IS MODAL COEFFICIENT FOR LOCATION i OF MODE r

U(J, r) IS MODAL COEFFICIENT FOR LOCATION j OF MODE r

FIGURE B-1

MODAL ASSURANCE CRITERION

$$MAC(c,d) = \frac{|MOM(c,d)|^2}{MOM(c,c)\ MOM(d,d)}$$

USED TO COMPARE MODE SHAPE'c TO MODE SHAPE d

$$MOM(c,d) = \sum_{j=1}^{m} a(c, j, r)\ a^*(d, j, r)$$

WHERE a_r IS A SINGLE TERM OF THE RESIDUE MATRIX (FOR MODE r) A

$$MOM(c,c) = \sum_{j=1}^{m} a(c, j, r)\ a^*(c, j, r)$$

c AND d ARE USED TO DESIGNATE COLUMNS OF THE RESIDUE MATRIX

$$MOM(d,d) = \sum_{j=1}^{m} a(d, j, r)\ a^*(d, j, r)$$

FIGURE B-2

SECONDARY STRUCTURE MODAL ASSURANCE CRITERIA

	1	2	3	4	5	6
1	1.00000	0.18024	0.00591	0.28021	0.18998	0.01536
2		1.00000	0.00191	0.18635	0.00053	0.01707
3			1.00000	0.00262	0.00014	0.11651
4				1.00000	0.00026	0.01316
5					1.00000	0.05288
6						1.00000

FIGURE B-3

APPENDIX C

APPENDIX C

RESIDUAL CORRECTIONS

Residual corrections have two applications. In the parameter estimation phase of modal test analysis, they serve to improve the quality of the curve fit, which is used to judge the quality of the parameter estimation. The second use if for a substructure coupling analysis, based on modal properties derived (by FEM or test) from a free-free structural configuration.

There are two types of residual corrections that can be made. The first is known as the residual inertance term. This term accounts for the rigid body motions of the free-free structure and can be used to estimate mass values of the structure. The second term is known as residual compliance (or sometimes as residual flexibility). The second term is used to estimate the effects of higher order terms. Figure C-1 illustrates the corrections on a FRF (taken from reference 3).

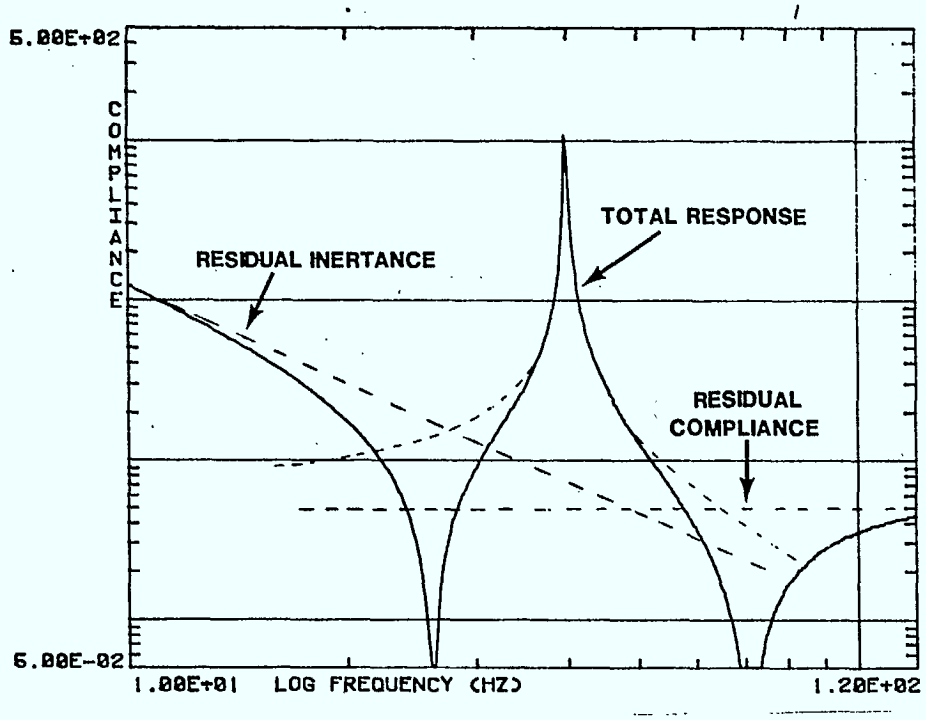

FIGURE C - 1

It has been shown (Klosterman, 1971) that the number of free-free modes needed for substructure coupling work is greater than the number of modes needed, if the coupling interface points are restrained. The use of a residual flexibility term reduces the number of free-free modes required.

The residual flexibility is obtained by applying a unit load at each of the interface points, generating the FRF and subtracting the amount of response which has been calculated from the modal characteristics. The best accuracy for this calculation is usually obtained near an anti-resonance in the modal response. (Klosterman, 1971)

The free-free case with a residual correction will be more suited for cases of relatively flexible interface connections than for very stiff ones.

APPENDIX D

```
 MACRO TO CORRECT BASE ACCELERATIONS
OM'INPUT FILE?';IS1
OM'OUTPUT FILE?';IS2
OM'REFERENCE COOR?';IC2;CRC2
XC2,6,7,8;V9=-V8;CC-2,V6,V7,V9
XM2;EM

LB1

   AH$1;IC1;XC1,2,3,4
JEV3,V7,4;OM'INCOR COOR DIR';OV3;EM
LB4;RHC1,1;V4=-V4;AA1,#V4
QH1,1,C2;AH$2;WH1;OM'MORE FUNCTS? YES=0';IV5
JEV5,0,1;EM

#
```



```
MACRO TO CONVERT STRAINS TO FORCES

LM1;LM2;LM3
OM'INPUT FILE';IS1
OM'OUTPUT FILE';IS2
 M'COORDINATE DOF S,E.G. 20X,20Y,20Z;';IC-1,2,3
OM'COORD TO BE CALC;';OC1,OC2,OC3
OM'ENTER CALIBRATION FACTORS?';IV2,3,4,5,6,7,8,9,10


'IF GAUGES USED ARE 2ND SET, TYPE 1;OTHERWISE 0';IV15;EM

OM'THE CALIBRATION MATRIX IS;'
OM'                          '; OV2,OV3,OV4
OM'                          '; OV5,OV6,OV7
OM'                          '; OV8,OV9,OV10
XM3;EM

V1=1;/U;V15=1-V15;V13=1


10;AH$1;RHCV1,V1;V12=V13+V1;V14=VV12;MAV1,#V14
IB1,10,4;AA2,1,2;AA2,3,2;JE15,20,0;QH2,5,5,;QH2,2,CV15
AH$2;WH2
LB20;V15=V15+1;V1=1;V13=V12-V1
IB13,10,10;EM

#
```

DRAISEY, SHERRY
--Modal test of T-Sat